

A collage of small planets from the Lick Carnegie Exoplanet Survey :
Exploring the super-Earth and sub-Neptune mass regime*

JENNIFER BURT,¹ FABO FENG,^{2,3} BRADFORD HOLDEN,⁴ ERIC E. MAMAJEK,⁵ CHELSEA X. HUANG,^{6,7}
MICKEY M. ROSENTHAL,⁸ SONGHU WANG,⁹ R. PAUL BUTLER,¹⁰ STEVEN S. VOGT,⁴ GREGORY LAUGHLIN,¹¹
GREGORY W. HENRY,¹² JOHANNA K. TESKE,^{10,13} SHARON X. WANG,¹⁴ JEFFREY D. CRANE,¹⁵ AND STEVE A. SHECTMAN¹⁵

¹*Jet Propulsion Laboratory, California Institute of Technology, 4800 Oak Grove drive, Pasadena, CA, 91109, USA*

²*Tsung-Dao Lee Institute, Shanghai Jiao Tong University, 800 Dongchuan Road, Shanghai 200240, People's Republic of China*

³*Department of Astronomy, School of Physics and Astronomy, Shanghai Jiao Tong University, 800 Dongchuan Road, Shanghai 200240, People's Republic of China*

⁴*UCO/Lick Observatory, Department of Astronomy and Astrophysics, University of California at Santa Cruz, Santa Cruz, CA, 95064, USA*

⁵*Jet Propulsion Laboratory, California Institute of Technology, 4800 Oak Grove Drive, Pasadena, CA, 91109, USA*

⁶*Department of Physics and Kavli Institute for Astrophysics and Space Research, Massachusetts Institute of Technology, Cambridge, MA, 02139, USA*

⁷*Juan Carlos Torres Fellow*

⁸*Department of Astronomy and Astrophysics, University of California, Santa Cruz, CA, 95064, USA*

⁹*Department of Astronomy, Indiana University, Bloomington, IN, 47405, USA*

¹⁰*Earth and Planets Laboratory, Carnegie Institution for Science, 5241 Broad Branch Road, NW, Washington, DC, 20015, USA*

¹¹*Department of Astronomy, Yale University, New Haven, CT, 06511, USA*

¹²*Center of Excellence in Information Systems, Tennessee State University, Nashville, TN, 37209, USA*

¹³*NASA Hubble Fellow*

¹⁴*Department of Astronomy, Tsinghua University, Beijing 100084, People's Republic of China*

¹⁵*Observatories of the Carnegie Institution for Science, 813 Santa Barbara St., Pasadena, CA, 91101, USA*

(Accepted October 13th, 2020)

Submitted to The Astronomical Journal

ABSTRACT

Analysis of new precision radial velocity (RV) measurements from the Lick Automated Planet Finder (APF) and Keck HIRES have yielded the discovery of three new exoplanet candidates orbiting two nearby K dwarfs not previously reported to have companions (HD 190007 and HD 216520). We also report new velocities from both the APF and the Planet Finder Spectrograph (PFS) for the previously reported planet host stars GJ 686 and HD 180617 and update the corresponding exoplanet orbital models. Of the newly discovered planets, HD 190007 b has a period of 11.72 days, an RV semi-amplitude of $K = 5.64 \pm 0.55 \text{ m s}^{-1}$, a minimum mass of $16.46 \pm 1.66 M_{\oplus}$, and orbits the slightly metal-rich, active K4 dwarf star HD 190007 ($d = 12.7 \text{ pc}$). HD 216520 b has an orbital period of 35.45 days, an RV semi-amplitude of $K = 2.28 \pm 0.20 \text{ m s}^{-1}$, and a minimum mass of $10.26 \pm 0.99 M_{\oplus}$, while HD 216520 c has an orbital period of $P = 154.43$ days, an RV semi-amplitude of $K = 1.29 \pm 0.22 \text{ m s}^{-1}$, and a minimum mass of $9.44 \pm 1.63 M_{\oplus}$. Both of these planets orbit the slightly metal-poor, inactive K0 dwarf star HD 216520 ($d = 19.6 \text{ pc}$). We find that our updated best fit models for HD 180617 b and GJ 686 b are in good agreement with the previously published results. For HD 180617 b we obtain an orbital period of 105.91 days, an RV semi-amplitude of $K = 2.696 \pm 0.224 \text{ m s}^{-1}$, and a minimum mass of $12.214 \pm 1.05 M_{\oplus}$. For GJ 686 b we find the orbital period to be 15.53 days, the RV semi-amplitude to be $K = 3.004 \pm 0.180 \text{ m s}^{-1}$, and the minimum mass to be $6.624 \pm 0.432 M_{\oplus}$. Using an injection-recovery exercise, we find that HD 190007 b and HD 216520 b are unlikely to have

Corresponding author: Jennifer A. Burt
jennifer.burt@jpl.nasa.gov

* This paper includes data gathered with the 6.5 meter Magellan Telescopes located at Las Campanas Observatory, Chile.

additional planets with masses and orbital periods within a factor of two, in marked contrast to $\sim 85\%$ of planets in this mass and period range found with Kepler.

Keywords: Exoplanet astronomy (486), Exoplanet systems (484), Radial velocity (1332)

1. INTRODUCTION

The use of precision ground-based Doppler spectrometers enabled the first generation of exoplanet detections, producing 47 exoplanet detections before the first exoplanet was discovered to transit in 1999 (Henry et al. 1999, 2000). Since then an additional 773 planets have been discovered using such instruments, bringing the total number of radial velocity (RV) detected planets to 820 as of September 2020¹.

More recently, numerous precision RV instruments have been spending more time pursuing targeted mass measurements of transiting planets discovered by space-based missions like *K2* and *TESS*. Such planets, for which we can obtain both mass and radius measurements, are valuable additions to the field as they enable studies of planetary composition and evolution (Burt et al. 2020; Christiansen et al. 2017; Teske et al. 2018, see e.g.). However more traditional Doppler surveys, which focus on repeated observations of nearby stars without any *a priori* knowledge of whether or not they host planets, are still a key component in our efforts to understand the Galaxy’s exoplanet population. Because RV detections do not require an exoplanet to transit its host star, an alignment that happens with only a few percent probability for even promising short period planets (Winn 2010), this method is sensitive to a wider range of orbital configurations. As such, many of our constraints on the characteristics and occurrence rates of long-period gas and ice giant planets come from RV surveys (Rowan et al. 2016; Bryan et al. 2019). And unlike transit observations, which detect planets during their fleeting inferior conjunctions, RV observations permit the planetary signal to build in the data over the entire span of observing time so they do not suffer as badly from short-term weather closures or varied observing times/locations. Examples of such surveys include the Lick Carnegie Exoplanet Survey (LCES, Butler et al. 2017, hereafter B17), the California Planet Search (CPS, Howard et al. 2010), the HARPS search for southern extra-solar planets (Pepe et al. 2004), and the CARMENES search for exoplanets around M dwarfs (Reiners et al. 2018).

While they are less susceptible to short-term disruptions, RV surveys are more observationally expensive

than transit surveys, requiring both long exposure times to reach the required high S/N levels on high-resolution spectrometers and long observing baselines to properly fill out a planet’s RV phase curve. This combination means that surveys often require months or years of data on a star before any potential planet signals are interpreted as robust detections. Additionally, RV surveys can often begin by selecting stars that seem promising based on their V magnitudes, effective temperatures (T_{eff}), rotational velocities, and $\log R'_{\text{HK}}$ activity indicators, only to learn months or years later that the stars are actually too active to allow for the detection of Keplerian signals that are only a few m s^{-1} in amplitude. When such stars are ultimately dropped from a survey, however, there is often no public record of the discontinuation of RV monitoring, nor is there a write up of *why* the star was excluded. This can result in future surveys observing that same target again, and spending many nights of telescope time only to realize once again that the star is not well-suited to RV science. Dropping targets also has strong, detrimental impacts on efforts to infer RV planet population statistics and makes it difficult to draw robust conclusions about planet occurrence rates from most RV surveys.

In 2017 the LCES team released a compendium of all the Keck HIRES RV observations acquired since the advent of the survey in 1994, resulting in 64,949 radial velocities spread over 1,624 stars in B17. The majority of stars included in the survey have V magnitudes between 6 and 10, with a median value of $V = 8$. Stars brighter than 5th magnitude were handled by the Hamilton spectrograph on the Shane 3m telescope at Lick Observatory. Observing times were limited to roughly 10 minutes per target per night in order to accommodate a relatively large target list which led to a faint magnitude limit of about 14th magnitude. The stellar spectral types covered by the survey run from about F5V to M6V. Stars hotter than F5V were generally avoided due to the decrease in RV information content (Bouchy et al. 2001; Beatty & Gaudi 2015) while stars cooler than M6V were generally past the faint end of the survey’s magnitude limit. For new or ongoing planet search surveys, the ability to sift through two decades of archival data and use it for either initial target selection or in combination with recent RV observations to search for potential Keplerian signals (or trends that could indicate notable

¹ <https://exoplanetarchive.ipac.caltech.edu>

stellar activity cycles which can last many years) is a powerful tool.

In this work, we make use of the LCES RV catalog as the backbone for two new planet detections and updated fits for two recently published planets. Two of these stars are among the 357 found in B17 to have significant signals that are of constant period and phase, but not coincident in period and/or phase with stellar activity indices in the original catalog publication. The other two display significant RV periodicities only after the HIRES velocities have been combined with RV data from other observatories. We begin in §2 with an overview of the specifics of each step of our analysis methods, as they are shared between the four stellar data sets. Then we detail the characteristics of exoplanet host stars and present a compilation of their stellar parameters in §3. Next, we cover each star and its associated planet detection individually in §4-7 before concluding in §8 with a discussion about how these planets compare to the multi-planet systems discovered in large part by the *Kepler* mission.

2. OVERVIEW OF DATA AND METHODOLOGY

Each star is analyzed using the same methodology and series of steps, which we summarize here. The initial data product for each target is a set of time series radial velocity measurements and the corresponding spectral activity indicators from various PRV instruments which are monitored using the interactive SYSTEMIC Console (Meschiari et al. 2009) over the months/years that the stars spend on our survey target lists. When the RV data sets show signs of a significant signal, we then work to determine whether or not the signal could have been caused by our observing approach or by the host star itself via chromospheric activity and/or stellar rotation (see, e.g., Rajpaul et al. 2016). To this end we first compute the spectral window function of the RV data sets to ensure the signal is not due to our observational cadence. We then gather, when available, long baseline photometric measurements to try and measure the stars’ rotation periods via seasonal changes in stellar brightness. We also derive S- and H-index activity indicators (described in §2.4) from the RV spectra to map the stars’ chromospheric activity signatures. And finally we assess the consistency of any signals over time by computing a moving periodogram with a moving average noise model (MA(1) model, described in §2.3) for those signals whose orbital phases are well-covered by the RV data. If none of these analyses produce signals that can explain the signature seen in the RV data, we then test whether the signal originally noted with SYSTEMIC is “significant” under a full Bayesian treatment

as seen in Feng et al. (2019). If so, we assume the signal is caused by a planet in orbit around the host star, and fit a Keplerian model to determine the exact parameters of the planet and its orbit. Additional details on each of these steps follow below.

2.1. Radial velocities

The data sets presented in this work consist of unbinned radial velocity observations taken with seven different instruments; the Levy spectrometer (on the 2.4m Automated Planet Finder telescope, Vogt et al. 2014), the High Resolution spectrometer (HIRES, on the 10m Keck I telescope, Vogt et al. 1994), the Planet Finder spectrometer (PFS, on the 6.5m Magellan Clay telescope, Crane et al. 2006, 2008; Crane 2010), the High Accuracy Radial Velocity Planet Searcher (HARPS, on the ESO 3.6m telescope, Mayor et al. 2003), the High Accuracy Radial velocity Planet Searcher for the Northern hemisphere (HARPS-N, on the 3.58m Telescopio Nazionale Galileo, Cosentino et al. 2012), the Spectrographe pour l’Observation des PHénomènes des Intérieurs stellaires et des Exoplanètes (SOPHIE, on the 1.93m reflector telescope at the Haute-Provence Observatory, Bouchy et al. 2011), and the CARMENES spectrometer (on the 3.5 m telescope at the Calar Alto Observatory, Quirrenbach et al. 2018). Samples of the velocities used in our analyses are presented in the appendix, while the full data sets will be made available as machine readable tables.

The APF, HIRES, and PFS RV values are all measured by placing a cell of gaseous I₂ in the converging beam of each telescope. This imprints the 5000-6200Å region of incoming stellar spectra with a dense forest of I₂ lines that act as a wavelength calibrator and provide a proxy for the point spread function (PSF) of each spectrometer. To ensure a constant I₂ column density over multiple decades, the cells are held at a constant temperature of 50.0 ± 0.1°C. The instruments have typical spectral resolutions of 90,000, 60,000 and 80,000 for the APF, HIRES and PFS, respectively. While only the 5000-6200Å spectral region is used for measuring radial velocities, the instruments produce spectra from 3700-7700Å for the APF, 3700-8000Å for HIRES, and 3900-6700Å for PFS.

Once the iodine region of the spectrum has been extracted, it is split into 2Å chunks. Each chunk is analyzed using the spectral synthesis technique described in Butler et al. (1996), which deconvolves the stellar spectrum from the I₂ absorption lines and produces an independent measure of the wavelength, instrument PSF, and Doppler shift. The final Doppler velocity from a given observation is the weighted mean of the veloci-

ties of all the individual chunks (~ 700 for the APF and HIRES, and ~ 800 for PFS). The final internal uncertainty of each velocity is the standard deviation of all 700 chunk velocities about that mean.

In contrast, HARPS, HARPS-N, and SOPHIE make use of multiple observing fibers, one of which is placed on the stellar target while the other is pointed at a Th-Ar calibration lamp to provide a simultaneous wavelength reference. The two HARPS instruments operate in the same region of wavelength space, from 3800-6900Å, and have the same peak resolving power of $\sim 115,000$ (Pepe et al. 2002; Cosentino et al. 2012). SOPHIE covers the same wavelength range as the two HARPS instruments, but has a slightly lower resolution of $\sim 75,000$.

The HARPS-TERRA velocities presented here are measured using the approach laid out in Anglada-Escudé & Butler (2012), using data obtained from the HARPS instrument described above. Specifically, the spectra for these observations are downloaded from the ESO archive and then each observation is decomposed into 1) a high signal-to-noise template, 2) the RV shift for that observation, and 3) a multiplicative background set of polynomials to account for flux variations. TERRA first derives approximate RVs measured against an observed spectrum and then improves the template by co-adding all observed spectra and recomputing the RVs. The spectra are co-added via a weighted least-squares regression with a cubic B-spline.

For the HARPS-N velocities the data reduction and spectral extraction were carried out using the Data Reduction Software (DRS v3.7). Once an observation is complete a 2-D spectra is optimally extracted from the resulting FITS file. The spectrum is cross-correlated with a numerical mask corresponding to the appropriate spectral type (F0, G2, K0, K5, or M4), and the resulting cross-correlation function (CCF) is fit with a Gaussian curve to produce radial velocity measurement (Baranne et al. 1996; Pepe et al. 2002) and calibrated to determine the RV photon-noise uncertainty σ_{RV} . The SOPHIE radial velocities are calculated using a similar data-reduction pipeline, which is adapted from the HARPS DRS software.

The CARMENES spectrometer consists of two cross-dispersed echelles and also employs multiple observing fibers in order to obtain simultaneous stellar and wavelength calibration data. The first spans 5200-9600Å in the visible (VIS) at a resolution of 94,600, while the second covers 9600-17100 Å in the near infrared (NIR) at a resolution of 80,400 (Quirrenbach et al. 2014). CARMENES makes use of the spectrum radial velocity analyser (SERVAL) software package to produce radial velocity measurements (Zechmeister et al. 2018). SER-

VAL is based upon the least-squares fitting approach described above and again computes precision RV measurements using a least-squares matching of each observed spectrum to a high signal-to-noise ratio template derived from the same observations.

2.2. Photometry and stellar rotation

To search for evidence of a given star’s stellar rotational period, we have acquired high-precision, long-baseline photometric data of HD 190007, GJ 686, and HD 180617 taken with the T12 0.8m and T4 0.75m APTs at Fairborn Observatory in the Stromgren *b* & *y* pass bands. The two-color observations have been combined to produce a $\Delta(b + y)/2$ joint-filter time series, which improves measurement precision. Program stars on these telescopes have their observations interlaced with three nearby comparison stars in the sequence: dark, A, B, C, D, A, SKYA, B, SKYB, C, SKYC, D, SKYD, A, B, C, D, where A, B, and C are the comparison stars and D is the program star. Integration times are 20-30 seconds (depending on stellar brightness) on the 0.75 m APT, where the Stromgren *b* & *y* observations are made sequentially, and 40 seconds on the 0.80 m APT, where the two bands are measured simultaneously (Henry 1999). The photometric data for each target and the resulting conclusions drawn from the data set is described in each star’s respective section of the paper.

2.3. Bayesian search and orbital fitting

The significance of signals initially identified with SYSTEMIC are assessed by calculating likelihood ratios and Bayes factors based on the Bayesian information criterion (e.g., Liddle 2007; Feng et al. 2016) and by applying a noise model that accounts for the most important sources of variability in a radial velocity time-series (Feng et al. 2016), i.e. Keplerian signals, an unknown amount of white noise, different unknown levels of correlated noise and potential linear correlations between velocities and available spectroscopic activity proxies. The model has been discussed in great detail in e.g. Feng et al. (2016, 2017a); Díaz et al. (2018).

The model for a given star’s RV solution is made up of a combination of signal and noise components, where the signal for N_p planets in the k^{th} RV data set is given by Equation 1:

$$\hat{v}_s^k(t_j) = \sum_{i=1}^{N_p} K_i [\sin(\omega_i + \nu_i(t_j)) + e_i \cos \omega_i] + \gamma_k + \dot{\gamma}_k t_j \quad (1)$$

where K_i is the RV semi-amplitude of stellar variation induced by the i^{th} planet’s gravitational pull on the

host star, $\nu_i(t_j)$ is the true anomaly derived from the planet’s orbital period P_i , eccentricity e_i and the reference mean anomaly M_0 after solving Kepler’s equation. Unlike [Feng et al. \(2019\)](#), we do not include a linear trend in the model as in some cases we find evidence of signals with periods approaching the RV data time span. We therefore replace the linear trend by an offset to avoid introducing degeneracies between potential long-period Keplerian signals and a linear trend term in the model.

We assess each RV dataset to determine whether it is best represented by a white noise model (a constant jitter is used to fit excess noise), or a moving average model (MA(1), [Tuomi et al. 2013](#)). In order to determine the order, q , of the MA model we calculate the maximum likelihood for a MA model using the Levenberg-Marquardt (LM) optimization algorithm. We calculate $\ln(\text{BF})$ for MA($q+1$) and MA(q). If $\ln(\text{BF}) < 5$, we select MA(q). If $\ln(\text{BF}) > 5$, we select MA($q+1$) and keep increasing the order of MA model until the model with the highest order passing the $\ln(\text{BF}) > 5$ criterion is found. Additional details on this model determination process can be found in [Feng et al. \(2019\)](#).

Once the appropriate model has been determined, we search for periodic signals in the data by applying an adaptive Metropolis algorithm [Haario et al. \(2006\)](#) combined with a parallel tempering scheme designed by [Feng et al. \(2019\)](#). This Markov-chain Monte Carlo technique has been applied to similar data sets (e.g. [Butler et al. 2017](#); [Vogt et al. 2017](#); [Tuomi et al. 2018](#)) and found to identify significant signals reliably with a low sensitivity to false positives ([Dumusque et al. 2017](#)). A signal is considered to be strong if the logarithmic Bayes factor is larger than 3 (i.e. $\ln(\text{BF}) > 3$) or equivalently its Bayesian information criterion (BIC) is larger than 6 ([Kass & Raftery 1995](#)). A signal is considered to be very strong or significant if $\ln(\text{BF}) > 5$. The exact number of free parameters needed for the RV fit is unknown, however, as a circular Keplerian model has three free parameters while an eccentric Keplerian orbit requires five. We therefore define $k = 3$ and $k = 5$ as the boundaries for the real BIC value, which are represented in the fit summaries as $\ln(\text{BF}_3)$ and $\ln(\text{BF}_5)$, respectively. Since we are using a sinusoidal model in the calculation of the BFPs, we use $\ln(\text{BF}_3) = 5$ as the initial threshold for declaring a signal to be significant. Although a more conservative criterion of $\ln(\text{BF}) > 6.9$ is proposed by [Nelson et al. \(2020\)](#), we keep using $\ln(\text{BF}) > 5$ in order to be consistent with the threshold proposed by [Kass & Raftery \(1995\)](#) and suggested by [Feng et al. \(2016\)](#) through analyses of RV data sets. Nevertheless, the results presented in this work are not sensitive to

the choice of $\ln(\text{BF})$ criteria because all planets satisfy the more conservative $\ln(\text{BF}) > 6.9$ criterion. The real significance of a signal, however, is determined through posterior sampling combined with the BF thresholds. This analysis is visualized by creating a $\ln(\text{BF})$ periodogram (BFP) for each of the individual RV data sets, in addition to a BFP for the combined RV data set.

In an attempt to identify those signals caused by stellar activity, we calculate BFPs for the activity indices and the observational window function for each data set and perform visual inspections to determine whether they exhibit overlapping periods with potential planetary signals in the RV data sets. To assess the consistency of signals over time, we compute a moving periodogram for those signals whose phase is well covered by the RV data. Since the RVs are typically not measured in a uniform way, the consistency of a true signal may depend on the sampling cadence even if the power is normalized. However, it is easy to identify false positives if inconsistency is found at high cadence epochs with a timescale comparable with or longer than the signal period ([Feng et al. 2019](#)).

A full set of white noise, moving average, and autoregressive BFPs for each target star’s RV data sets, activity indicators, and window function is presented in Appendix 1.

2.4. Stellar activity indicators

The derived spectral activity indicators from each of our HIRES, PFS, and APF spectra serve as proxies for chromospheric activity in the visible stellar hemisphere at the moments when the spectra were obtained. The S-index is obtained from measurement of the emission reversal at the cores of the Fraunhofer H and K lines of Ca II located at 3968 Å and 3934 Å, respectively ([Duncan et al. 1991](#)).

For the APF data, we employ an adaptation of the S-index analysis presented in [Isaacson & Fischer \(2010\)](#) where, for each star, we identify the observation with the highest SNR level as the “reference spectrum” and then compute the redshift of that spectrum by cross correlating with the NSO solar atlas. All other spectra are then shifted into the same reference frame and continuum aligned to that reference spectrum using 10Å continuum regions in order to remove flux differentials arising from different SNRs between the exposures. The flux in the Ca II H & K bands and their associated continuum bands are measured and recorded, and the final data sets are calibrated against the original Mt. Wilson S-index survey results to allow for comparisons with our Keck and PFS data.

We also report H-index measurements for our APF, PFS, and post-fix (taken after the detector upgrade in August 2004) HIRES spectra. Similarly to the S-index, the H-index quantifies the amount of flux within the H α Balmer line core compared to the local continuum. Details on the prescription used for the HIRES and PFS data sets can be found in [Butler et al. \(2017\)](#). For the APF, we use the [Gomes da Silva et al. \(2011\)](#) prescription, which defines the H-index as the ratio of the flux within $\pm 0.8\text{\AA}$ of the H α line at 6562.808\AA to the combined flux of two broader flanking wavelength regions: $6550.87 \pm 5.375\text{\AA}$ and $6580.31 \pm 4.375\text{\AA}$. The H-index measurements often show peaks at periods of roughly one year due to the presence of shallow telluric lines that can shift into and out of the H α filter if the star’s systemic radial velocity places them on the edge of the H α line. We find that attempts to remove these lines change the shape and flux level of the H α line in substantial ways that compromise the search for flux modulations indicative of stellar activity. Therefore we do not remove the tellurics, but rather search for additional signals in the H-index periodograms after removing the one-year cycles.

For the HARPS data sets, which we process through the HARPS TERRA pipeline, we also make use of the Ca II H & K activity indicators that TERRA measures, in addition to the line bisectors (BIS), full width half max (FWHM), and CCF which are taken from the original HARPS DRS results.

We analyze the resulting activity indicators by computing Bayes factor periodograms for each activity indicator in each RV data set and looking for any well-defined peaks with $\ln(\text{BF}_5) > 5$ at or near the period of our suspected planets. In cases where we see peaks in these regions, we then compute the correlation coefficients between the RV measurements and the activity indicator measurements to look for evidence that the stellar activity is influencing the star’s radial velocities.

3. STELLAR PARAMETERS

All four stellar hosts described herein are nearby, dwarf stars with spectral types from K0V to M3V. These stars make excellent candidates for traditional iodine cell-based RV spectrometers thanks to their relatively bright V magnitudes and abundance of narrow absorption lines in the visible part of the spectrum ([Burt et al. 2015](#)). These stars in particular were selected for inclusion in the long running Lick-Carnegie Exoplanet Survey (LCES) carried out in B17 using Keck HIRES after analysis of early spectra revealed them to be chromospherically inactive and slowly rotating - two other key characteristics for RV candidates. Two of the stars (HD

190007 and HD 216520) do not have previously known exoplanets, which often prompts in-depth study of stellar characteristics. Their proximity to Earth and resulting bright magnitudes, however, have lead to their inclusion in a number of different surveys and large stellar characterization efforts (see, e.g., [Lépine & Gaidos 2011](#); [Mann et al. 2015](#); [Brewer et al. 2016](#)) that provide us with the parameters for each star presented in Table 1. The stars have also been examined by [Mishenina et al. \(2013\)](#), which provides individual elemental abundances (Table 2). For the other two targets with previously published planets (GJ 686 and HD 180617) we take the stellar parameters from [Schweitzer et al. \(2019\)](#).

4. HD 190007

HD 190007 (GJ 775, HIP 98698) is a nearby ($12.714 \pm 0.010\text{ pc}$)², relatively bright ($V = 7.46$; [ESA 1997](#)), K4V(k) star ([Gray et al. 2006](#), ; see summary of parameters in Table 1) The star is a moderately active star showing elevated chromospheric emission via Ca H & K ($\log R'_{\text{HK}} = -4.652$) ([Olsperg et al. 2018](#)) and coronal X-ray emission ($\log L_X/L_{\text{bol}} = -4.98$) ([Hinkel et al. 2017](#)). HD 190007 was classified as a BY Dra variable and designated V1654 Aql in the General Catalogue of Variable Stars (GCVS) by [Kazarovets et al. \(2003\)](#) based on the observed photometric variability reported by [Lockwood et al. \(1997](#), ; b -band amplitude of 0.016 mag). BY Draconis variables are usually K or M-type dwarfs that display quasiperiodic photometric variations on timescales of hours to months with amplitudes from 1-500 mmag that are believed to be driven by surface spots and chromospheric activity (e.g. [López-Morales et al. 2006](#)). While the eponymous star BY Dra itself is a close binary ($P = 6$ days), and many BY Dra stars are close binaries, the manifestations of magnetic activity (starspots, strong emission lines) are tied to relatively rapid rotation ([Bopp & Espenak 1977](#)). The star’s level of chromospheric and coronal activity, and observed amplitude of photometric variability (e.g. [Mamajek & Hillenbrand 2008](#); [Radick et al. 1998](#)), appears to be normal for a mid-K dwarf with its rotation period of $P_{\text{rot}} = 28.626 \pm 0.046$ days (Table 1, Section 4.3). The published T_{eff} estimates mostly cluster between $\sim 4500\text{ K}$ and 4700 K (see Table 3) and we adopt $T_{\text{eff}} = 4610 \pm 20\text{ K}$.

Previous analyses of the star show good agreement on HD 190007 being slightly metal-rich (e.g., $[\text{Fe}/\text{H}] = 0.14 \pm 0.06$ ([Ramírez et al. 2012](#)), 0.16 ± 0.05 ([Mishenina](#)

² $\varpi = 78.6238 \pm 0.0617\text{ mas}$ ([Gaia Collaboration et al. 2018](#)), and distance calculated as $1/\varpi$, including parallax zero point shift from [Lindgren et al. \(2018\)](#).

Table 1. Stellar parameters

Parameter	HD 190007	HD 216520	GJ 686	HD 180617
Right Ascension	20 02 47.05 ^a	22 47 31.88 ^a	17 37 53.35 ^a	19 16 55.26 ^a
Declination	03 19 34.27 ^a	83 41 49.30 ^a	18 35 30.16 ^a	05 10 08.04 ^a
Spectral type	K4V(k) ^b	K0V ^c	M1.0V ^d	M2.5V ^d
ϖ (mas)	78.6238 ± 0.0617 ^a	51.1167 ± 0.0292 ^a	122.5609 ± 0.0346 ^a	169.1590 ± 0.0520 ^a
Distance (pc)	12.72 ± 0.01 ^a	19.56 ± 0.011 ^a	8.159 ± 0.0023 ^a	5.912 ± 0.0018 ^a
Systemic RV (km s ⁻¹)	-30.467 ± 0.133 ^a	-18.536 ± 0.182 ^a	-10.092 ± 0.232 ^a	35.554 ± 0.158 ^a
V	7.46 ^e	7.53 ^e	9.62 ^e	9.12 ^e
G	7.0634 ^a	7.2790 ^a	8.7390 ^a	8.0976 ^a
M_V	6.94 ± 0.01 ^{a,e}	6.08 ± 0.02 ^{a,e}	10.04 ± 0.03 ^{a,e}	10.26 ± 0.005 ^{a,e}
M_G	6.54 ^{a,e}	5.82 ^{a,e}	9.18 ^{a,e}	9.24 ^{a,e}
$B - V$	1.128 ± 0.015 ^e	0.867 ± 0.010 ^e	1.530 ± 0.015 ^e	1.464 ± 0.005 ^e
$B_p - R_p$	1.3534 ^a	1.0496 ^a	2.1173 ^a	2.3816 ^a
K_s	4.796 ± 0.017 ^f	5.449 ± 0.021 ^f	5.572 ± 0.020 ^g	4.673 ± 0.020 ^g
Mass (M_\odot)	0.77 ± 0.02 ^{tw}	0.82 ± 0.04 ^{tw}	0.426 ± 0.017 ^d	0.484 ± 0.019 ^d
Radius (R_\odot)	0.79 ± 0.039 ⁱ	0.760 ± 0.007 ^{tw}	0.427 ± 0.013 ^d	0.481 ± 0.014 ^d
log Luminosity (L/L_\odot)	-0.68 ± 0.01 ^j	-0.452 ± 0.004 ^{tw}	-1.53 ± 0.011 ^d	-1.49 ± 0.0052 ^d
[Fe/H]	0.16 ± 0.05 ^k	-0.16 ^h	-0.23 ± 0.16 ^d	-0.04 ± 0.16 ^d
T_{eff} (K)	4610 ± 20 ^{tw}	5103 ± 20 ^{tw}	3656 ± 51 ^d	3534 ± 51 ^d
log(g) (cm s ⁻²)	4.58 ± 0.02 ^l	4.54 ± 0.028 ^h	4.87 ± 0.07 ^d	4.90 ± 0.07 ^d
P_{rot} (days)	28.626 ± 0.046 ^[tw]	unknown	38.732 ± 0.286 ^[tw]	50.60 ± 0.41 ^[tw]
$v \sin i$ (km s ⁻¹)	2.55 ^m	0.2 ± 0.5 ^h	2.49 ⁿ	<2 ^p
RV data	APF, HIRES	APF, HIRES	APF, HIRES, PFS HARPS, HARPS-N SOPHIE, CARMENES	APF, HARPS HIRES CARMENES

NOTE— ^aGaia Collaboration et al. (2018), ^bGray et al. (2006), ^cGray et al. (2003), ^dSchweitzer et al. (2019), ^eESA (1997), ^fCutri et al. (2003), ^hBrewer et al. (2016), ⁱKervella et al. (2019), ^jBiazzo et al. (2007), ^kMishenina et al. (2013), ^lFranchini et al. (2014), ^mMishenina et al. (2012), ⁿHoudebine et al. (2016), ^pReiners et al. (2018), ^[tw]this work,

et al. 2013)), similar to the well-studied Hyades cluster (Fe/H \simeq 0.15-0.18 Dutra-Ferreira et al. 2016; Cummings et al. 2017; Liu et al. 2016). This metallicity enhancement likely explains why the star is slightly above the Main Sequence in B-V vs. M_V space ($dM_V \sim -0.16$) (Isaacson & Fischer 2010). An upper limit on the ages of thin-disk stars this metal-rich is roughly <8 Gyr (Mishenina et al. 2013).

The star has multiple published mass estimates, compiled in Table 3, however we complement these values with some new independent estimates based on luminosity and absolute magnitude. The star has metallicity similar to the Hyades cluster, which has [Fe/H] \simeq +0.18 (Dutra-Ferreira et al. 2016) and an age of $\sim 700 \pm 100$ Myr (Brandt & Huang 2015; Martín et al. 2018; Gossage et al. 2018; Lodieu et al. 2019). Torres (2019) has found that stars in eclipsing binaries in the Hyades show reasonable agreement in their mass versus abso-

lute magnitude trend against the PARSEC evolutionary tracks (Chen et al. 2014) for [Fe/H] = +0.18 and 625-800 Myr isochrones. Using the Chen et al. (2014) isochrone matched to the Hyades, the absolute magnitude ($M_V = 6.94$) corresponds to mass 0.774 M_\odot . K dwarfs evolve very slowly, and indeed a 5 Gyr isochrone for the same chemical composition yields mass 0.756 M_\odot for the same M_V . Using the mass-luminosity trend for main-sequence stars from Eker et al. (2018) yields a mass estimate of 0.772 M_\odot . If one fits a quadratic³ to the absolute magnitudes vs. log(mass) for the well-characterized FGK

³ $\log_{10}(M/M_\odot) = 0.4391 - 0.107645 M_V + 3.818613e-3 M_V^2$. The fit is appropriate for FGK dwarfs (although anchored to late A's and early M's) over $1.6 < M_V < 9.0$. The RMS scatter is about 5.7% and likely dominated by the differences in chemical abundances and ages among the field dwarfs in the Torres (2010) review.

Table 2. Stellar Abundances from [Mishenina et al. \(2013\)](#)

Species	HD 190007	HD 216520
[Fe/H]	0.16	-0.17
[O/Fe]	-0.16	0.20
[Mg/Fe]	-0.11	0.09
[Si/Fe]	0.10	0.01
[Ca/Fe]	0.13	0.02
[Ni/Fe]	0.03	-0.07
[Y/Fe]	-0.06	-0.13
[Zr/Fe]	-0.19	0.00
[Ba/Fe]	-0.03	-0.20
[La/Fe]	-0.18	-0.12
[Ce/Fe]	-0.20	0.00
[Nd/Fe]	-0.16	0.07
[Sm/Fe]	-0.15	0.08
[Eu/Fe]	-0.04	0.09

NOTE—Based on discussion in [Mishenina et al. \(2008, 2013\)](#) the abundance uncertainties are on the order of ± 0.06 dex for Fe, Mg, and Si, ± 0.1 dex for O, Ca, and Ni, and ± 0.1 - 0.15 dex for Y, Zr, Ba, La, Ce, Nd, Sm, and Eu.

dwarf detached binaries compiled in the review by [Torres \(2010\)](#), for $M_V = 6.94$ one would predict $0.752 \pm 0.043 M_\odot$. The distribution of mass estimates is tightly clustered in [Table 3](#) and we simply adopt $M_\star = 0.77 \pm 0.02 M_\odot$ based on the mean and standard deviation (representing the scatter among multiple methods to derive the mass).

Multiple independent age estimates can be made using the star’s rotation and activity indicators. Using the X-ray age calibrations from [Mamajek & Hillenbrand \(2008\)](#) we estimate an X-ray age estimate of 0.9 Gyr, which is in general agreement with previously published ages from X-rays (1.08 Gyr, [Vican 2012](#)), rotational age-dating (1.5 ± 0.3 Gyr and 2.0 ± 0.4 Gyr from [Ramírez et al. 2012](#); [Aguilera-Gómez et al. 2018](#), respectively), and high resolution visible spectra (0.88 Gyr, [Kóspál et al. 2009](#)). However, recent results from *Kepler* and *K2* studies of young clusters show that the rotational evolution of K dwarfs shows significant stalling between ages of ~ 0.7 and 1 Gyr, and that a Skumanich-like rotational evolution law is a poor approximation ([Curtis et al. 2019](#)). Comparing the star’s combination of color ($B_p - R_p = 1.3534$ [Gaia Collaboration et al. 2018](#)) or T_{eff} , and rotation period, to young clusters and field dwarfs in the *Kepler* field ([Curtis et al. 2019](#)), we find that the star is clearly older than 1 Gyr, and its age is likely typical for field stars in the *Kepler* field.

Variations in published RVs show evidence of a linear trend on the order of 0.5 km s^{-1} over ~ 16 years

Table 3. T_{eff} and M_\star Estimates for HD 190007

T_{eff} (K)	Reference
4352 ± 70	Houdebine (2012)
4466	Katz et al. (2011)
4541^{+80}_{-43}	Boeche & Grebel (2016)
4568 ± 23	Houdebine et al. (2019)
4571 ± 117	Bai et al. (2019)
4596 ± 40	Luck (2017)
4597 ± 8	Franchini et al. (2014)
4599 ± 85	Ramírez et al. (2012)
4603 ± 91	Aguilera-Gómez et al. (2018)
4611 ± 40	González Hernández & Bonifacio (2009)
4616 ± 10	Stevens et al. (2017)
4637 ± 51	Casagrande et al. (2006)
4640 ± 51	Casagrande et al. (2010)
4650	Luck & Heiter (2005)
4681 ± 1	Biazzo et al. (2007)
4709	Anders et al. (2019)
4722	Stassun et al. (2018)
4724 ± 7	Mishenina et al. (2008)
4724	Frasca et al. (2015)
4610 ± 20	adopted T_{eff}
$M_\star (M_\odot)$	Reference
0.80	Wright et al. (2011)
0.785 (0.773-0.801)	Takeda et al. (2007)
0.778 ± 0.039	Kervella et al. (2019)
0.774	a
0.772	b
0.76	Luck (2017)
0.760 ± 0.091	Stassun et al. (2018)
0.752 ± 0.043	c
0.751 (0.732-0.801)	Anders et al. (2019)
$0.73^{+0.03}_{-0.01}$	Ramírez et al. (2012)
0.77 ± 0.02	adopted M_\star

NOTE— a) from [Chen et al. \(2014\)](#) isochrone matching Hyades ($[\text{Fe}/\text{H}]=0.18$, $Z=0.0193$, $\log(\text{age}/\text{yr}) = 8.85$), following [Torres \(2019\)](#). b) using luminosity-mass calibration from [Eker et al. \(2018\)](#). c) from fit of M_V to mass for FGK dwarfs for detached binary stars compiled by [Torres \(2010\)](#).

that could be due to a stellar or sub-stellar companion ([Soubiran et al. 2013](#)). HD 190007 does not, however, show evidence of a significant tangential velocity anomaly ($dV_t = 13.89 \pm 8.16 \text{ m s}^{-1}$) nor an abnormally high Gaia DR2 RUWE value (RUWE = 0.89), either of which would lend additional support to the possibility of a binary companion ([Kervella et al. 2019](#); [Gaia Collaboration et al. 2016](#)). HD 190007 has not previ-

ously been the target of high resolution imaging efforts to look for stellar companions using the VLT (NACO or SPHERE) or Gemini (using GPI, NIRC2, or NIRC1), nor has it been targeted by Robo-AO. Such observations may help clarify the trend seen in the previously published radial velocity data and we encourage such follow up efforts.

Based on its Gaia DR2 results, we find that HD 190007 has a barycentric galactic velocity of $U = -22.097 \pm 0.006$ km s^{-1} , $V = -16.461 \pm 0.006$ km s^{-1} , $W = 15.442 \pm 0.007$ km s^{-1} with U measured towards the Galactic center, V in the direction of Galactic rotation, and W towards the North Galactic Pole (ESA 1997). Adopting the Local Standard of Rest (LSR) from Bland-Hawthorn & Gerhard (2016) gives $U_{LSR} = -12.1$ km s^{-1} , $V_{LSR} = -5.5$ and $W_{LSR} = 22.4$ km s^{-1} , for a total LSR velocity of 26.1 km s^{-1} . Following the kinematic selection criteria of Bensby et al. (2014), we estimate kinematic membership probabilities of $P_{thin} = 98.74\%$, $P_{thick} = 1.26\%$, $P_{halo} = 0.0003\%$, and the probability of membership in the Hercules dynamical stream as $P_{Hercules} = 0.00007\%$. Mackereth & Bovy (2018) calculates that HD 190007’s Galactic orbit has 3D pericenter and apocenter radii of 6.998 and 8.103 kpc, respectively, an eccentricity of 0.07306 and a maximum vertical excursion of 0.336 kpc. The star’s Banyan Σ , a Bayesian classification tool that identifies members of young moving groups, yields $P_{field} = 99.9\%$ independent of whether the star’s default RV or Gaia DR2 RV is used - so it does not appear to belong to any known nearby young moving groups (Gagné et al. 2018).

We use the measured abundances for the α elements Mg, Si, and Ca, and the Fe abundance from Mishenina et al. (2013) to estimate the α enrichment $[\alpha/\text{Fe}]$ (e.g. Bovy 2016). Adopting unweighted means of the abundances of three α elements with respect to iron, we estimate $[\alpha/\text{Fe}] \simeq 0.04$. Similarly, Franchini et al. (2014) estimate $[\alpha/\text{Fe}] = 0.03 \pm 0.01$. These kinematic calculations and abundance ratios suggest that the star is a metal-rich thin disk star (e.g. Mishenina et al. 2013).

HD 190007 will not be surveyed during the primary mission of NASA’s *TESS* satellite, which would have allowed for more detailed characterization of the star’s brightness modulations, due to its proximity to the Earth and Moon contamination zone that the *TESS* observing plan has been shifted to avoid.

4.1. HD 190007 Radial velocities

The RV data set for HD 190007 contains observations from two instruments, HIRES on Keck I and the APF’s Levy spectrometer. The Keck data is comprised of 34 unbinned velocities (32 individual epochs) obtained from

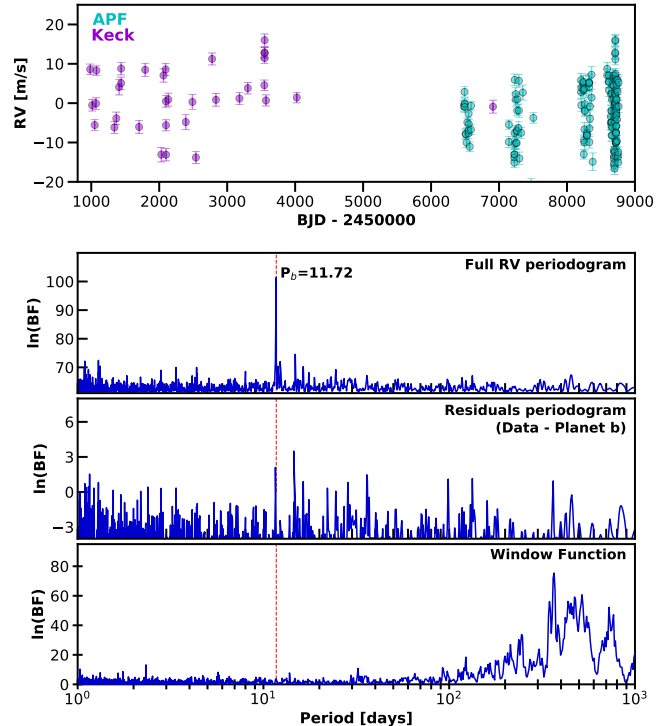


Figure 1. First panel: Unbinned radial velocity measurements of HD 190007 taken with the APF (cyan), and Keck HIRES (purple). Second panel: Bayes factor periodogram of the RV data showing the potential planet peak at 11.72 days. Third panel: Bayes factor periodogram of the RV residuals after the 11.72 day signal has been modeled and removed. Fourth panel: Spectral window function of the combined RV data sets.

June 1998 - September 2014 with a mean internal uncertainty of 1.54 m s^{-1} . The APF data is comprised of 157 unbinned velocities (91 individual epochs) obtained from July 2013 - October 2019 with a mean internal uncertainty of 1.50 m s^{-1} . Analysis of the combined data set reveals a prominent peak at 11.72 days (Figure 1).

To discern whether this signal could be caused by non-planetary sources, we first examine the spectral window function of the combined data set (Figure 1). Notable peaks in the window function - such as the peak at $P=1.0$ d that results from night time observing restrictions - can cause aliases to appear at $f_{alias} = f_{planet} + f_{WF}$ (Dawson & Fabrycky 2010). None of the periods that we would expect from this star’s combined window function show up prominently in the 11-12 day range of the RV periodogram, and thus we do not suspect observational aliases of masquerading as the 11.72 day signal.

4.2. HD 190007 Activity indicators

Only seven observations of HD 190007 were taken with Keck HIRES after the detector upgrade that expanded

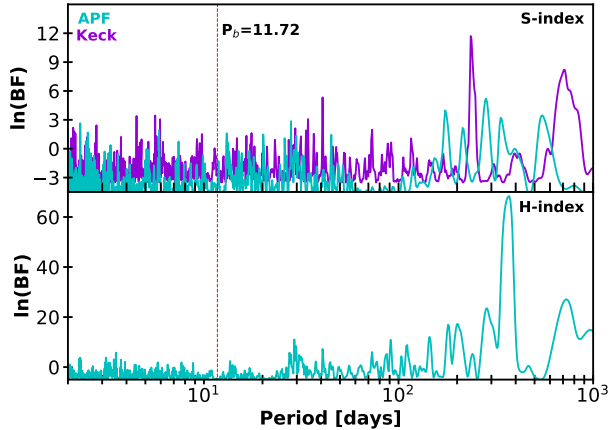


Figure 2. Top: Bayes factor periodogram of the S-index values measured from the APF and Keck HIRES data sets in cyan and purple, respectively. Bottom: Same as above, but for the H-index measurements extracted from the APF data. In both panels there are no prominent peaks in the vicinity of the proposed planet period of 11.72 days, but there is a broad activity-based peak at 29.18 days that is likely tied to rotational modulation evident in the APF activity indicators. The Keck HIRES data set contains only 6 observations able to produce H-index measurements, which is insufficient to produce an informative periodogram.

HIRES’ wavelength range and enabled measurement of the H α line, which is not a large enough data set to compute a meaningful Bayes factor periodogram. None of the periodograms of the three available activity data sets (S- and H-index from the APF, and S-index from HIRES) show peaks at or near the proposed 11.72 day planet period (Figure 2). Based on the lack of notable signals at periods matching our potential planet signal, we conclude that the 11.72 day signal is not due to the varieties of stellar activity that produce variance in the emission of the Ca II H&K and H α spectral features.

The APF S- and H-index measurements show evidence of a relatively broad signal with period, $P \sim 29.18$ days which we take to be a sign of rotational modulation due to its close match with the stellar rotation period as identified in Section 4.3. Fitting a Keplerian model to this long term signal produces a best fit period of $P = 29.180 \pm 0.012$ days and an RV semi-amplitude of $K = 3.54 \pm 0.90 \text{ m s}^{-1}$ (Figure 3). While we believe the signal to be due to stellar variability and not an additional planet, as the signal does not appear with significant power in the combined RV periodogram, we still included the signal in our overall RV model of the system.

4.3. HD 190007 Photometry and stellar rotation

A total of 1092 observations were obtained over 21 observing seasons, spanning 1997 through 2017 using the T4 0.75-m APT at Fairborn Observatory. The compar-

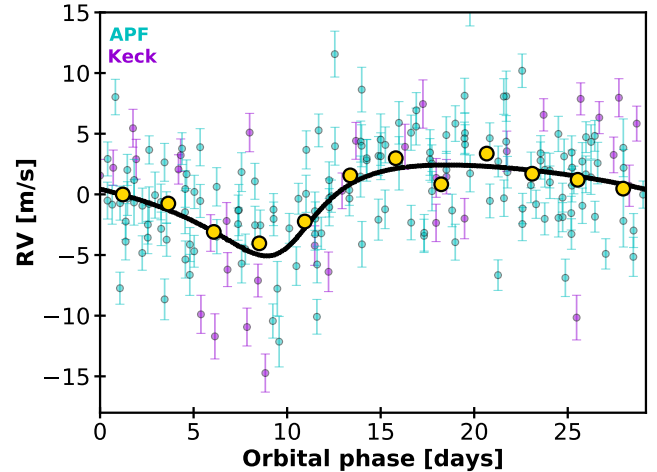


Figure 3. RV observations of HD 190007 phase folded to the best fit period of the suspected rotational activity cycle, $P_{\text{act}} = 29.18$ days, with APF observations shown in cyan and Keck HIRES observations shown in purple. The error bars include the excess white noise “jitter” from our analysis, and the black solid curve denotes the maximum a posteriori Keplerian model. Yellow points depict the phase-binned RV data.

ison stars used in the data analysis are HD 190521, (a K0III star with $V = 7.60$, $B-V = 1.15$) and HD 187406 (an F3V star with $V = 7.67$, $B-V = 0.48$). The photometry shows that HD 190007 varies from year to year by roughly ~ 0.016 mag. When searching the data for rotation periods, we find significant signals in all seasons except those covering 1999 and 2001. The star does, however, appear to be “double spotted” in the years 2000, 2002, 2006, and 2015. In these cases, the rotation period is twice the observed photometric period. Analyzing the 19 seasons where we measure rotational periods, we derive a weighted- mean rotation period of 28.626 ± 0.046 days (Figure 4), which is well separated from the proposed planet periods of 11.72 days but overlaps closely with the ~ 29 day signal seen in the APF activity indicators. This rotation period is also in agreement with the $P_{\text{rot}} = 27.68 \pm 0.36$ day derived in Olsperg et al. (2018).

4.4. HD 190007 Orbital parameters

Having concluded that neither our observing scheme, the star’s chromospheric activity, nor the star’s rotation could be causing the 11.72 day signal we observe in HD 190007’s RV periodogram, we move on to testing whether or not the RV data provide enough Bayesian evidence to support the existence of the suspected planet. We apply a statistical model accounting for Keplerian signals and red noise, as well as correlations between radial velocities and activity data (see Section 2).

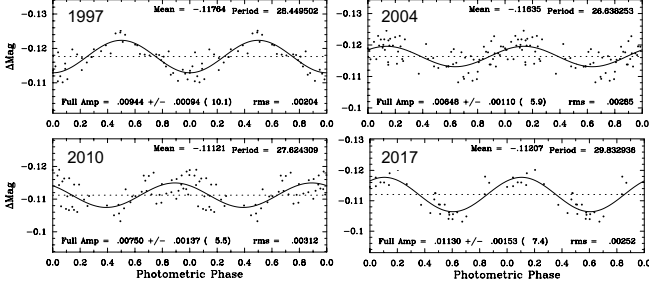


Figure 4. A selection of four of the 19 seasons of photometry in which HD 190007 displayed a significant rotation signal. Analyzing the combined set of 19 seasons of rotational periods, we derive a weighted-mean rotation period of 28.626 ± 0.046 days, which is in general agreement with the 29.18 day activity signal measured using the APF S- and H-index activity indicators.

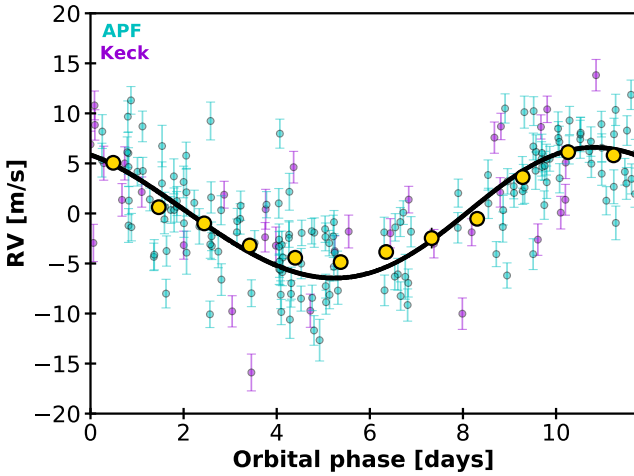


Figure 5. RV observations of HD 190007 phase folded to the best fit period of $P = 11.72$ days, with APF observations in cyan and Keck HIRES observations in purple. The error bars include the excess white noise “jitter” from our analysis, and the black solid curve denotes the maximum *a posteriori* Keplerian model. Yellow points depict the phase-binned RV data.

The resulting fit to the data reveals a planet with a period of 11.72 days, a semi-amplitude of $K = 5.64 \text{ m s}^{-1}$, and an eccentricity of $e = 0.14$ (Figure 5, Table 5). This corresponds to a $16.46 M_{\oplus}$ planet orbiting 0.092 AU from its host star. The signal is detected at $\ln(\text{BF}_5) = 29.2$, well above the $\ln(\text{BF}_5) = 5$ limit we set for identifying a signal as statistically significant. Thus we promote the 11.72 day signal to being labeled as a newly identified planet candidate, HD 190007 b.

5. HD 216520

HD 216520 (HIP 112527) is a $V=7.53$, K0V star (Gray et al. 2003) located 19.6 parsecs away in the con-

stellation of Cepheus ($\varpi = 51.1167 \pm 0.0292$ mas; Gaia Collaboration et al. 2018). The metallicity of the star has been estimated in several studies, with values ranging between $[\text{Fe}/\text{H}] = -0.22$ and -0.14 , with median value $[\text{Fe}/\text{H}] = -0.17$, i.e. slightly metal poor (Brewer et al. 2016; Luck 2017; Mishenina et al. 2008, 2012; Mikolaitis et al. 2019). Effective temperature and mass estimates for HD 216520 are shown in Table 4. We adopt the recent T_{eff} value from Luck (2017), whose value (5130 ± 20 K) falls near the middle of a tight cluster of recent estimates from high resolution spectroscopy surveys including Mishenina et al. (2008); Bermejo et al. (2013); Brewer et al. (2016); Luck (2017) and Mikolaitis et al. (2019).

We calculate the bolometric luminosity using the Virtual Observatory SED Analyzer (VOSA)⁴ from (Bayo et al. 2008). We use VOSA to query archival UV/Vis/IR photometry from several sources (GALEX, Tycho, Gaia DR2, 2MASS, WISE)⁵ and fit synthetic stellar spectra in order to constrain the star’s bolometric flux and independently check the T_{eff} estimates. We find a best fit BT-Settl-CIFIST model (constraining $\log(g) = 4.5$ and solar metallicity) with 5100 K, which has bolometric flux $f_{\text{bol}} = 2.949 \times 10^{-8}$ ($\pm 1\%$) $\text{erg cm}^{-2} \text{s}^{-1}$ ($m_{\text{bol}} = 7.33 \pm 0.01$ on the IAU 2015 bolometric scale). Combined with the Gaia DR2 parallax, we estimate the absolute bolometric magnitude to be $M_{\text{bol}} = 5.87 \pm 0.01$, and the luminosity to be $\log(L/L_{\odot}) = -0.452 \pm 0.004$. Combining this luminosity estimate with our adopted T_{eff} value yields an estimated radius of $0.760 \pm 0.007 R_{\odot}$. This is similar to recent estimates by Brewer et al. (2016) ($0.79 \pm 0.02 R_{\odot}$), Stassun et al. (2019) ($0.794 \pm 0.043 R_{\odot}$), and Gaia Collaboration et al. (2018) ($0.77^{+0.01}_{-0.02} R_{\odot}$). All of these radii estimates are systematically smaller than that predicted in the JMMC Stellar Diameter Catalog (JSDC) (Version 2; Chelli et al. 2016; Bourges et al. 2017), which estimates an angular diameter of $\theta_{LD} = 0.3989 \pm 0.0093$ mas (and when combined with the Gaia DR2 parallax yields a radii estimate of $0.839 \pm 0.020 R_{\odot}$). In Table 4 we list several published mass estimates and three new independent ones based on the the estimates of the star’s luminosity and absolute magnitude. We adopt a mass of $0.82 \pm 0.04 M_{\odot}$ for HD 216520, which spans the range of masses estimated using evolutionary tracks and empirical trends.

⁴ <http://svo2.cab.inta-csic.es/theory/main/>

⁵ GALEX: Bianchi et al. (2017), Tycho: ESA (1997), 2MASS: Cutri et al. (2003), WISE: Cutri & et al. (2012). Gaia DR2 photometry was omitted as it led to large uncertainty (0.2) in the derived bolometric magnitude.

Measurements of the star’s chromospheric activity through the Ca H & K S-index and $\log R'_{\text{HK}}$ indices show the star to be relatively inactive, indeed similar to that of the Sun. Isaacson & Fischer (2010) report 124 epochs of Ca H & K measurements, showing the star’s activity ranging from $\log R'_{\text{HK}} = -4.860$ to -5.006 . These values span a range not too much wider than that observed over typical solar cycles (indeed almost identical to that seen over solar cycle 19; Egeland 2018). Using the rotation-activity-age relations from Mamajek & Hillenbrand (2008), the mean $\log R'_{\text{HK}}$ value from Brewer et al. (2016) (-4.93) is consistent with the star’s Rossby number being 2.02, with a predicted rotation period of 43 days and an age of ~ 6.7 Gyr. Previous estimates based on chromospheric activity by Wright et al. (2004) and Isaacson & Fischer (2010) similarly estimated ages and predicted rotation periods of 5.25 Gyr/44.0 day and 5.19 Gyr/42 day, respectively. Isochronal age estimates incorporating the star’s HR diagram constraints and metallicity and using several different sets of evolutionary tracks by Luck (2017) spanned 4.84 ± 2.81 Gyr.

Based on its Gaia DR2 results, we find that HD 216520 has a heliocentric velocity of $U = 17.458 \pm 0.007 \text{ km s}^{-1}$, $V = -16.905 \pm 0.006 \text{ km s}^{-1}$, $W = 8.341 \pm 0.009 \text{ km s}^{-1}$ with U measured towards the Galactic center, V in the direction of Galactic rotation, and W towards the North Galactic Pole (ESA 1997). With respect to the LSR of Bland-Hawthorn & Gerhard (2016), the velocities are $U_{\text{LSR}} = +27.5 \text{ km s}^{-1}$, $V_{\text{LSR}} = -5.9 \text{ km s}^{-1}$, $W_{\text{LSR}} = +15.3 \text{ km s}^{-1}$, with overall LSR velocity of 32.0 km s^{-1} . Using the kinematic criteria of Bensby et al. (2014), we estimate kinematic membership probabilities for HD 216520 of for the thin disk, thick disk, halo, and Hercules dynamical stream of: $P_{\text{thin}} = 99.005\%$, $P_{\text{thick}} = 1.004\%$, $P_{\text{halo}} = 0.0002\%$, and $P_{\text{Hercules}} = 0.000007\%$. Mackey & Bovy (2018) calculate that HD 216520’s Galactic orbit has 3D pericenter and apocenter radii of 6.753 and 8.431 kpc, respectively, an eccentricity of 0.11, and a maximum vertical excursion of 0.224 kpc. Chemically and kinematically, the star is squarely consistent with being a member of the thin disk, corroborating previous classifications by Mishenina et al. (2013) and Hinkel et al. (2017). The star’s lithium abundance, $\log A(\text{Li}) = -0.30$ (Mishenina et al. 2012), sets a lower age limit of roughly 0.5 Gyr. Note that the combination of chromospheric activity and metallicity/kinematic constraints show that the isochronal age of 11.1 Gyr as listed by Brewer et al. (2016) (6.9-13.8 Gyr) seems unlikely. Based on the available constraints from chromospheric activity measurements, isochronal age estimates, and Galactic kinematic constraints, we adopt an age of 6 ± 3 Gyr.

Table 4. T_{eff} and M_{\star} Estimates for HD 216520

T_{eff} (K)	Reference
5082 ± 25	Brewer et al. (2016)
5103 ± 20	Luck (2017)
5119 ± 7.3	Mishenina et al. (2008)
5119 ± 50	Mikolaitis et al. (2019)
5140^{+59}_{-27}	Gaia Collaboration et al. (2018)
5156 ± 132	Bai et al. (2019)
5163 ± 72	Bermejo et al. (2013)
5103 ± 20	adopted T_{eff}
M_{\star} (M_{\odot})	Reference
0.78	a
0.79 ± 0.02	Brewer et al. (2016)
0.808 ± 0.040	Kervella et al. (2019)
0.84	b
0.84 ± 0.02	Luck (2017)
0.844 ± 0.049	b
0.850 ± 0.103	Stassun et al. (2019)
0.900 ± 0.045	Kervella et al. (2019)
0.82 ± 0.04	adopted M_{\star}

NOTE— a) Using Chen et al. (2014) isochrone for $[M/H] = -0.16$ for age 6 Gyr. b) using Eker et al. (2018) mass-luminosity trend for adopted luminosity. c) from fit of M_V to mass for FGK dwarfs for detached binary stars compiled by Torres (2010).

5.1. Radial velocities

The RV data set for HD 216520 contains observations from two instruments, Keck HIRES and the APF’s Levy spectrometer. The Keck data is comprised of 504 unbinned velocities (210 individual epochs) obtained from October 2001 - June 2017 with a mean internal uncertainty of 1.26 m s^{-1} . The APF data is comprised of 300 unbinned velocities (91 individual epochs) obtained from October 2014 - June 2020 with a mean internal uncertainty of 2.02 m s^{-1} .

Combining these data sets, we find two strong, well-defined peaks in the RV periodogram at periods of $P = 35.45$ and 154.43 days. When comparing this period with the data sets’ combined spectral window function, we find no corresponding alias peaks (Figure 6).

5.2. Activity indicators

Plotting the Bayes factor periodograms of the S-index values extracted from the APF and HIRES spectra for HD 216520 reveals a set of peaks in the 20-40 day period range in the Keck HIRES S-index and H- α data (see inset panels in Figure 7). Closer inspection shows that none of the HIRES activity peaks overlap directly with the suspected planet signal, and that the APF data

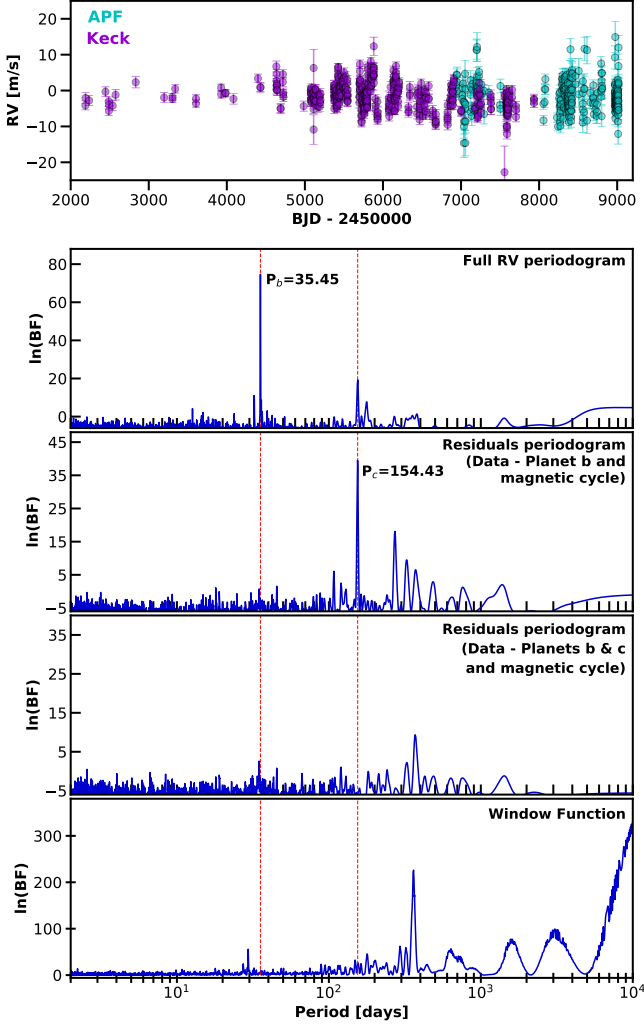


Figure 6. First panel: Unbinned radial velocity measurements of HD 216520 taken with the APF (cyan), and Keck HIRES (purple). Second panel: Bayes factor periodogram of the RV data showing the suspected planet peak at 35.45 days. Third panel: Bayes factor periodogram of the RV residuals after the 35.45 day Keplerian signal and the $\sim 7,700$ activity signal have been fit and removed from the data sets. The second suspected planet peak at 154.43 days is clearly visible. Fourth panel: Bayes factor periodogram of the RV residuals after both suspected planets and the activity signal have been modeled and removed. Fifth panel: Spectral window function of the combined RV data sets showing a lack of significant peaks that could cause alias signals at the period observed in the RVs.

does not show significant power in this period range, but given the proximity of the HIRES activity peaks we compare the HIRES RVs to their corresponding S- and H-index values and measure the Pearson correlation coefficients (PCC). The PCC values are 0.12 and 0.22 for the S- and H-index values, respectively, both of which fall below the $PCC > 0.30$ that is used as the threshold

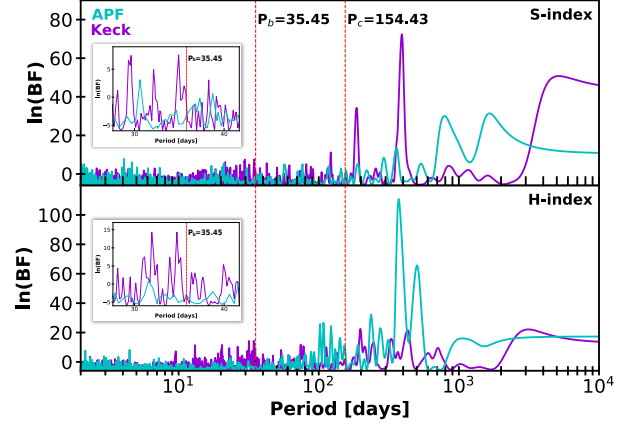


Figure 7. Top: Bayes factor periodogram of the S-index values measured from the APF and Keck HIRES data sets for HD 216520 in cyan and purple, respectively. Inset is a zoomed version focusing on the region around the suspected 35.45 day planet signal. Bottom: Same as above, but for the H-index measurements extracted from the APF and Keck HIRES data. The planet period does not overlap with any significant peaks in either the S-index or H-index periodogram.

for identifying a moderate linear relationship. These low PCC values suggest that the stellar variability mapped by the S- and H-index indicators is not driving periodicity within the RV data.

Both the HIRES S-index measurements and the combined HIRES and APF RV measurements show evidence of a signal with period, $P \sim 7700$ days which we take to be a long term magnetic activity cycle (see Figures 6, 7). The lack of this signal in the APF S-index periodogram is not surprising as the APF data set spans only 2081 days. Fitting a Keplerian model to this long term signal produces a best fit period of $P = 7767.35 \pm 1464.31$ days and an RV semi-amplitude of $K = 1.90 \pm 0.35 \text{ m s}^{-1}$ (Figure 8). While we believe the signal to be due to stellar variability and not an additional planet, given the overlap in periodicity seen in the combined RV and HIRES S-index data sets, we still included the signal in our overall RV model of the system.

5.3. Photometry and stellar rotation

HD 216520 was observed by NASA’s *TESS* mission (Ricker et al. 2014) during Sectors 18 (UT Nov 3 - 27 2019), 19 (UT Nov 28 - Dec 23 2019), and 20 (UT Dec 24 - Jan 21 2020). The star fell on Camera 3 during all three sectors, and on CCD 3 in sector 18 and CCD 4 in sectors 19 and 20.

The Science Processing Operations Center (SPOC) data (Jenkins et al. 2016) for HD 216520, available at the the Mikulski Archive for Space Telescopes (MAST)

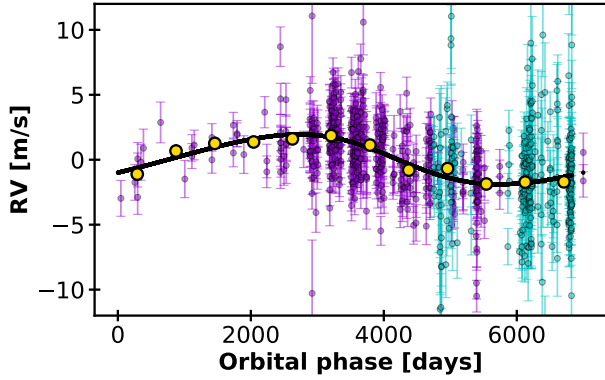


Figure 8. RV observations of HD 216520 phase folded to the best fit period of the long term activity cycle, $P_{\text{act}} = 7767.35$ days, with APF observations shown in cyan and Keck HIRES observations shown in purple. The error bars include the excess white noise “jitter” from our analysis, and the black solid curve denotes the maximum a posteriori Keplerian model. Yellow points depict the phase-binned RV data.

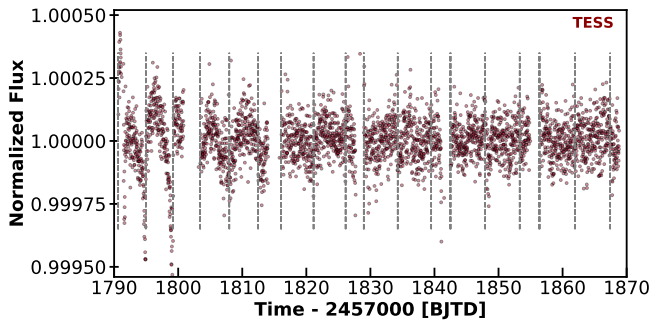


Figure 9. Top panel: Three sectors of presearch data conditioned simple aperture photometry (PDCSAP) flux measurements of HD 216520 taken with the *TESS* spacecraft. The 5 day periodicity seen in the light curve is caused by the spacecraft’s regularly scheduled momentum dumps. No signs of stellar periodicity are visible, leaving us unable to discern the star’s rotation period from the *TESS* data.

website⁶, includes the pre-search data conditioned simple aperture photometry (PDCSAP) flux measurements (Smith et al. 2012; Stumpe et al. 2012, 2014) shown in Figure 9. At the start of each orbit, thermal effects and scattered light can impact the systematic error removal in PDC (see *TESS* data release note DRN16 and DNR17). Therefore we have used the quality flags provided by SPOC to mask out unreliable segments of the time series.

While many of the instrumental variations present in the SAP flux are removed in the PDCSAP result, there

are still obvious signs of the spacecraft’s momentum dumps that occur on a roughly five day period. Beyond the five day periodicity, we do not see any evidence of rotational modulation in the *TESS* photometry. Given that HD 216520 has an estimated rotation period of 42–44 days based on its chromospheric activity indicators and rotation-activity-age relations (§ 5), we would expect to see almost two full rotations over the duration of the *TESS* data. The lack of evident rotation signals therefore further supports the theory that the star is relatively inactive, as suggested by its $\log R'_{\text{HK}}$ values.

5.4. Orbital parameters

Having established that neither our observational cadence, stellar activity, nor stellar rotation are likely to be the cause of the 35.45 day signal, we now test whether or not the combined RV data provides enough Bayesian evidence to support the existence of the suspect planet. We again apply a statistical model accounting for Keplerian signals and red noise, as well as for correlations between the radial velocities and the activity indicator data sets (see Section 2). We find that the 35.45 day signal is well-supported by the data, with a Bayes factor of $\ln(\text{BF}_5) = 35.37$, again well above the $\ln(\text{BF}_5) = 5$ criteria for being identified as a statistically significant signal.

The resulting fit to the data reveals a two planet system, where the inner planet has a period of 35.45 ± 0.011 days, a semi-amplitude of $K = 2.28 \pm 0.20 \text{ m s}^{-1}$, and an eccentricity of $e = 0.09 \pm 0.06$ while the outer planet has a period of 154.43 ± 0.44 days, a semi-amplitude of $K = 1.29 \pm 0.22 \text{ m s}^{-1}$, and an eccentricity of $e = 0.12 \pm 0.08$ (Figure 10, Table 5). This corresponds to a $10.26 \pm 0.99 M_{\oplus}$ planet on an $0.198 \pm 0.0004 \text{ AU}$ orbit and an $9.44 \pm 1.63 M_{\oplus}$ planet on an $0.528 \pm 0.010 \text{ AU}$ orbit, henceforth referred to as HD 216520 b and HD 216520 c, respectively.

To investigate the persistence of the proposed planetary signal over time, we create a Moving Periodogram (MP) using the MA(1) noise model of Feng et al. (2017b). The Moving Periodogram is made by constructing Bayesian periodograms for the HD 216520 radial velocity data within a moving time window (see Feng et al. 2017b, for a detailed description). In doing so, we find that the 35.45 day signal is detected robustly and repeatedly as more RV data points are added. Indeed, the signal is consistent through an observational baseline that covers more than 90 orbits of the suspected planet and more than 9 seasons of ground based RVs (Figure 11). If RV peaks are long-lived, and survive over numerous seasons of observation, then stellar activity is generally considered unlikely to be the source

⁶ <https://mast.stsci.edu>

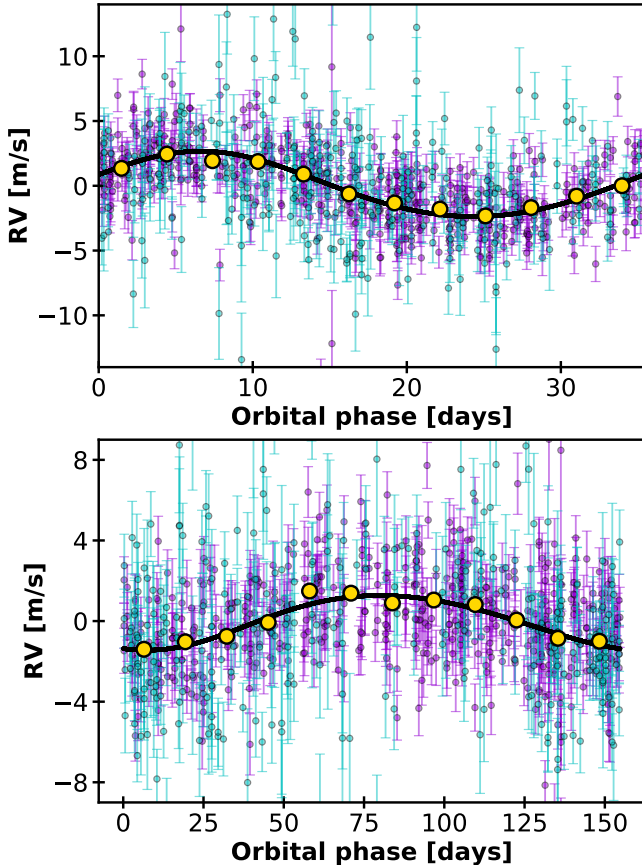


Figure 10. Top panel: RV observations of HD 216520 phase folded to the best fit period of planet b, $P_b = 35.45$ days, with APF observations shown in cyan and Keck HIRES observations shown in purple. Bottom panel: Same as above, but folded to the best fit period of planet c, $P_c = 154.43$ days. In both cases the error bars include the excess white noise “jitter” from our analysis, and the black solid curve denotes the maximum *a posteriori* Keplerian model. Yellow points depict the phase-binned RV data.

of the signal (see, e.g. Buchhave et al. 2016; Pinamonti et al. 2019). As the moving MP does not show evidence of the 35.45 day signal evolving over time nor show a broad distribution of period measurements over the decade long RV baseline, as we would expect were it caused by stellar variability, we take this as additional evidence that the signal is not due to surface variability on the host star.

5.5. Transit Search

Using the transit probability equation from Winn (2010) we calculate P_{tra} for each of the HD 216520 planet candidates. For planet b, $P_{\text{tra}} = 1.8\%$ while for planet c the probability drops to $P_{\text{tra}} = 0.6\%$. Given the planets’ best fit minimum masses ($10.26 M_{\oplus}$ and $9.44 M_{\oplus}$ for planets b and c, respectively) and the con-

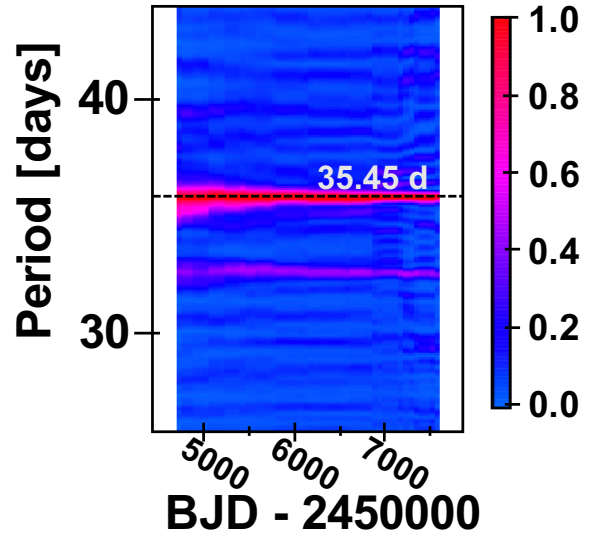


Figure 11. Moving MP-based periodogram for the combined HD 216520 radial velocity data sets. The colors encode the scaled MP power, which is truncated to optimize the visualization of signals. The suspected 35.45 day planet period is denoted with a horizontal dashed lines and shows robust detection through time bins encompassing more than 100 orbits.

ditional distributions for planet radius given a measured planet mass presented in Ning et al. (2018), we would expect these planets to have radii in the $2\text{--}4 R_{\oplus}$ range. A search of the three sectors of *TESS* data does not reveal signs of transits for either planet, neither via a traditional box least squares (BLS) search nor via phase folding the photometry at the best fit RV periods.

To test the likelihood that any potential transits may have been missed in the *TESS* data, we performed an injection and recovery experiment to determine if we could detect these planets assuming they do transit (Figure 12). We use the period posterior derived from the RV data, and injected the transits into the SPOC PDCSAP lightcurves assuming a uniform distribution of epochs within the *TESS* baseline, and a uniform distribution of impact parameters. We injected planets over a grid of radii between 1.0 and $4 R_{\oplus}$, with a step size of $0.15 R_{\oplus}$. We then detrended the light curves using the Kepler spline (Vanderburg & Johnson 2014), and used the BLS method to search for the transits using the best fitted RV period. We define a detection of the injected planet if the signal is detected at the correct epoch and with a BLS pink noise to signal ratio larger than 10. For planet b, we are able to detect the planet more than 80% of the time when the planet radius is larger than $1.4 R_{\oplus}$. For planet c, we are able to detect the single transit more than 80% of the time when the planet radius is

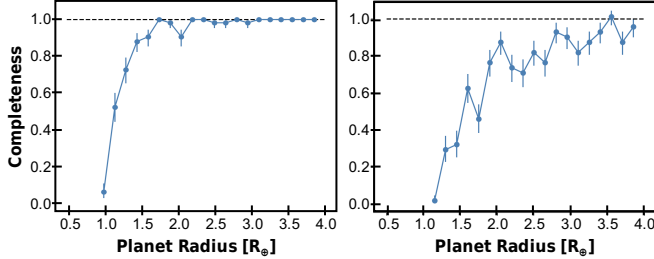


Figure 12. Results of our injection recovery analysis using the HD 216520 *TESS* data for planet b (left panel) and planet c (right panel). For planet b, we are able to detect the planet more than 80% of the times when the planet radius is larger than $1.4 R_{\oplus}$. For planet c, we are able to detect the single transit more than 80% of the times when the planet radius is larger than $2.0 R_{\oplus}$.

larger than $2.0 R_{\oplus}$. Given the expected planet radii, we therefore conclude that planet b does not transit, and that planet c did not transit during the observational baseline covered by the *TESS* photometry.

5.6. Dynamic Stability

A commonly used metric to assess the stability of two-planet systems is the separation of the planets in units of the mutual Hill radius

$$R_{H,\text{mut}} = \left(\frac{a_1 + a_2}{2} \right) \left(\frac{m_1 + m_2}{3M_*} \right)^{1/3} \quad (2)$$

where $m_{1,2}$ and $a_{1,2}$ are the masses and semi-major axes of the planets respectively, and M_* is the mass of the central star. Analytic calculations show that two low-eccentricity, low-inclination planets are “Hill stable,” meaning that they are protected from close encounters for all time, if their spacing in mutual Hill radii, $\Delta \equiv (a_2 - a_1)/R_{H,\text{mut}}$, exceeds $2\sqrt{3}$ (Gladman 1993; Chambers et al. 1996).

While this criterion is only approximate, the spacing between the HD 216520 planets indicates that stability is likely not a concern. Using MAP parameters, the mutual Hill radius between the two planets is $R_{H,\text{mut}} \approx 0.01$ au, giving a spacing in mutual Hill radii of $\Delta \approx 31.6$.

As another check, we used the N-body integration package *rebound* (Rein & Liu 2012) to integrate the system for 10^7 orbital periods of the outer planet, i.e. roughly 4.2 Myr. We employed the *whfast* integrator (Rein & Tamayo 2015), using a timestep of $0.01 \times$ (inner planet’s period). We see no indications of instability during the course of this integration. Over the course of the integration the variation in both planets’ semi-major axes is $< 10^{-5}$ au.

6. GJ 686

GJ 686 is a $V=9.62$ (ESA 1997) M1.5V (Lépine et al. 2013) star $d = 8.157 \pm 0.001$ pc away in Hercules ($\varpi = 122.5609 \pm 0.0346$ mas Gaia Collaboration et al. 2018) (Table 1)⁷. The star was recently reported to host an $m \sin i = 7.1 \pm 0.9 M_{\oplus}$ planet on a 15.53 day orbit by (Affer et al. 2019), and the signal was subsequently confirmed by Lalitha et al. (2019) ($m \sin i = 6.24_{-0.59}^{+0.58} M_{\oplus}$). Here we present an updated orbital analysis of the system that includes additional data taken with the APF and PFS, and present an updated minimum mass with 7% uncertainty.

6.1. Radial velocities

The previously published data sets for GJ 686 include 114 unbinned Keck HIRES velocities (90 individual epochs) from June 1997 - September 2013, 20 HARPS velocities (19 individual epochs) from June 2004 - September 2010, 25 SOPHIE velocities obtained from July 2007 to August 2009, 64 HARPS-N velocities obtained from February 2014 - October 2017, and 100 velocities obtained with the visible arm of CARMENES from February 2016 - November 2018. These data are described in detail in Affer et al. (2019) & Lalitha et al. (2019). To these, we add 134 unbinned APF velocities (59 individual epochs) taken from July 2013 - March 2016, and 18 PFS velocities (18 individual epochs) taken from August 2012 - March 2017. Additionally, we reprocess the HARPS data included in the previous papers using the TERRA pipeline (Anglada-Escudé & Butler 2012) before performing our own orbital fits. Searching the RV periodogram of the combined data set we find a strong, well defined peak at $P = 15.53$ days, matching the planet period found in the previously published works, and a lack of potential alias signals in the combined data’s window function (Figure 13). After removing the 15 day signal, we detect an additional signal with a period of $P \sim 2000$ days, which we (like Affer et al. (2019)) find to be evidence of a long-term activity cycle based on the Keck and APF activity indicators.

6.2. Photometry and stellar rotation

A total of 508 photometric observations were obtained over 7 observing seasons, spanning 2010 through 2016, using the T12 0.8m APT at Fairborn Observatory. The comparison stars used in our data analysis were HD 158806 (an F6IV star with $V = 6.92$, $B-V=0.46$) and HD 159063 (a G0V star with $V=6.98$, $B-V=0.53$). The photometry shows that GJ 686 varies from year to year by roughly $\sim 1\%$, consistent with low to moderate activity.

⁷ The proximity of GJ 686 was first reported and its parallax measured (108 ± 11 mas) by Slocum & Mitchell (1913).

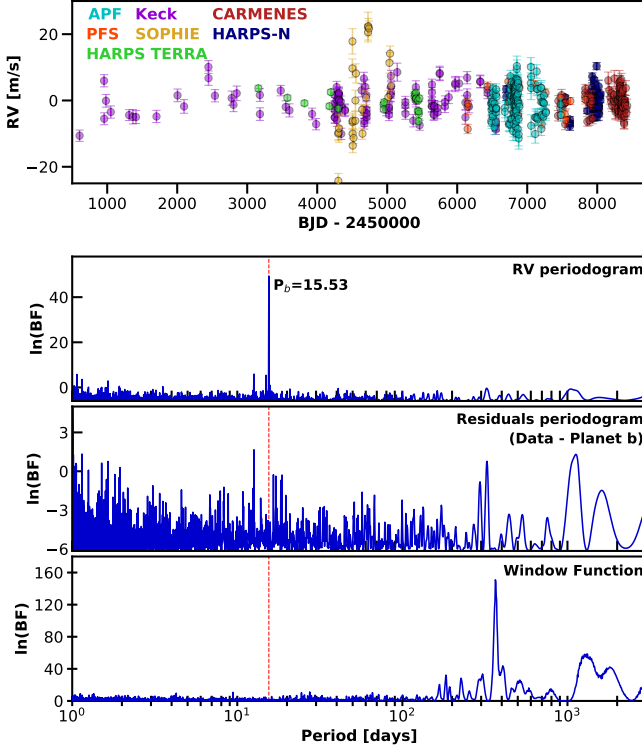


Figure 13. First panel: Unbinned radial velocity measurements of GJ 686 color coded by instrument. Second panel: Bayes factor periodogram of the RV data points showing the peak we detect at 15.53 days. Third panel: Residuals periodogram after the 15 day signal has been fitted and removed from the data. Broad peaks in the 1000-2000 day region remain. Fourth panel: Spectral window function of the combined RV data sets showing a lack of signals that could cause the 15.53 day signal.

When searching the photometric data for periodicity, we find significant signals only in the first four seasons. The star appears to be “double spotted” in 2011, cutting the observed photometric period in half. A weighted mean of the four photometric periods (doubling that from the 2011 observing season) gives us a value of 38.732 ± 0.286 days (Table 1, Figure 14), which we take to be our best estimate of the stellar rotation period. We note that this is well separated from our proposed new planetary period.

6.3. Activity indices

When plotting the S- and H-index Bayes factor periodograms using measurements extracted from our APF, HIRES, and PFS spectra for GJ 686, we find that none of the periodograms of the various activity data sets show peaks at or near the 15.53 day planet period (Figure 15). We do, however, see a peak at $P = 40.8$ days, which is in rough agreement with the stellar rotation period we measure, and those presented by Affer et al.

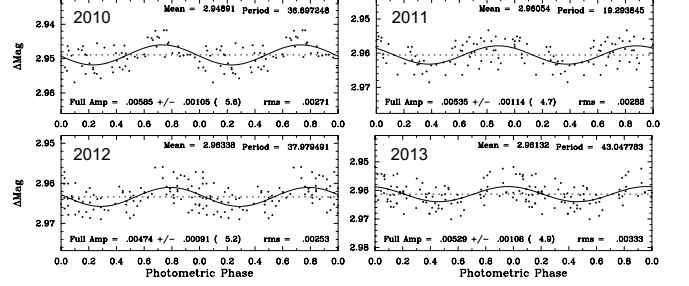


Figure 14. The first four years of GJ 686 photometry, in which we detect coherent rotation signals. From these four data sets we derive a weighted mean rotation period of 38.732 ± 0.286 days.

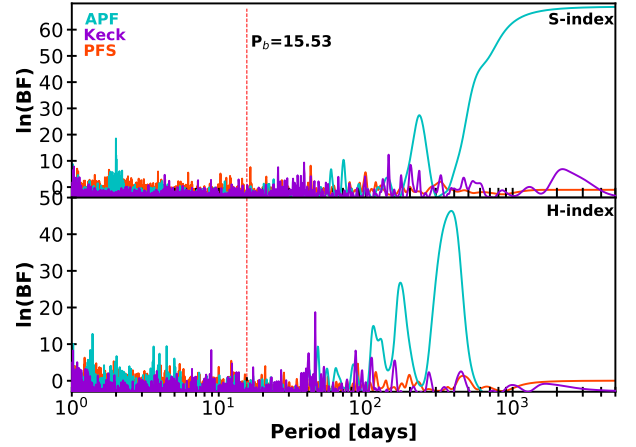


Figure 15. Top: Bayes factor periodogram of GJ 686 using the S-index values measured from the APF, Keck HIRES, and PFS data sets in cyan, purple, and orange, respectively. There are no prominent peaks in the vicinity of the 15.53 day planet period. Bottom: Same as above, but for the H-index measurements extracted from the Keck HIRES and PFS data in purple and orange, respectively.

(2019) ($P_{rot} = 36.7$ days) and Lalitha et al. (2019) ($P_{rot} = 38.4$ days). When considering the 2000 day signal, which the HIRES S-index data shows clearly at the $\ln(\text{BF}_5) \sim 10$ level, we note that of the individual stellar activity data sets only the Keck HIRES indicators covers a long enough time baseline to be sensitive to such a long-period sinusoid. We identify this signal as a likely long-period magnetic cycle, and with a period of ~ 5.5 years it aligns well with the typical long term variability timescales for early to mid M-dwarfs (Gomes da Silva et al. 2012; Suárez Mascareño et al. 2017).

6.4. Orbital parameters

Unsurprisingly, given its status as a previously published planet, we find that the 15.53 day signal is well supported by the combined RV data sets, with $\ln(\text{BF}_5) = 65.88$. The resulting fit to the data reveals a planet

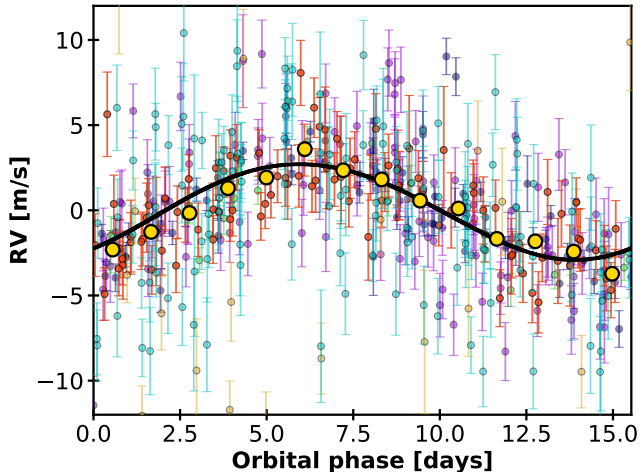


Figure 16. Top panel: RV observations of GJ 686 (colors match those in Figure 13) phase folded to the best fit period of $P = 15.53$ days. The error bars include the excess white noise “jitter” from our analysis, and the black solid curve denotes the maximum a posteriori Keplerian model. Yellow points depict the phase-binned RV data.

with a period of 15.53 days, a semi-amplitude of $K = 3.004 \text{ m s}^{-1}$, and an eccentricity of $e = 0.050$ (Figure 16, Table 5). This corresponds to a $6.624 M_{\oplus}$ planet orbiting 0.091 AU from its host star. These values are in good agreement with the previously published detections of GJ 686 b, and our RV semi-amplitude matches the smaller value measured in Lalitha et al. (2019) ($K=3.02^{+0.18}_{-0.20} \text{ m s}^{-1}$) more closely than the value measured by Affer et al. (2019) ($K=3.29^{+0.31}_{-0.32} \text{ m s}^{-1}$).

7. HD 180617 B

HD 180617 is an M3 dwarf star located just under six parsecs away from the Sun (Gaia Collaboration et al. 2016). The star was recently found to host a $12.2 m \sin i$ planet on a 105.9 day orbit using data from Keck HIRES, HARPS, and CARMENES (Kaminski et al. 2018). Here we present an updated orbital fit that incorporates an additional 126 radial velocity measurements taken with the APF between July 2013 and July 2019.

7.1. Radial velocities

The published RV data sets for this star include 158 unbinned HIRES velocities (134 individual epochs) taken from June 2001 to September 2014, 108 HARPS velocities taken before the fiber upgrade, 40 HARPS velocities taken after the fiber upgrade, and 124 CARMENES velocities. These RV data sets have mean uncertainties of 2.57, 0.85, 0.45, and 1.59 m s^{-1} , respectively, and are described in detail in Kaminski et al. (2018). The APF data included here is comprised of 126 radial velocity measurements (58 individual epochs)

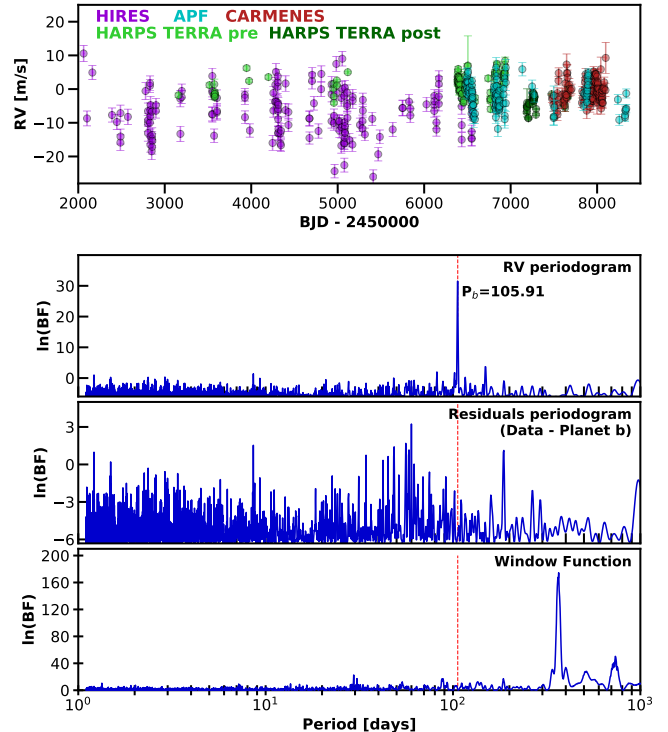


Figure 17. First Panel: Unbinned radial velocity measurements of HD 180617 taken with the APF (cyan), Keck HIRES (purple), and HARPS (green). Second Panel: Bayes factor periodogram of the RV data showing the planet’s peak at 105.91 days. Third panel: Residuals periodogram after the 105.91 day signal has been fitted and removed. Fourth panel: Window function of the combined RV data set showing a clear lack of significant peaks at the proposed planet period.

taken between July 2013 and July 2019 that have a mean uncertainty of 1.65 m s^{-1} . Searching the combined data set, we find a strong, well-defined peak in the RV periodogram at $P = 105.91$ days, which is consistent with the planet period detected in Kaminski et al. (2018), and a corresponding lack of signals in the combined RV window function that could cause the RV peak (Figure 17).

7.2. Activity indicators

S- and H-index activity indicators were extracted from each of the HIRES and APF spectra using the methods described in §2 (Figure 18). We find no significant peaks at the period of the planet ($P = 105.91$ days), however the data from the APF does include large peaks at ~ 200 days, which match a peak seen in indicators sensitive to line-profile variations described in Kaminski et al. (2018).

7.3. Photometry and stellar rotation

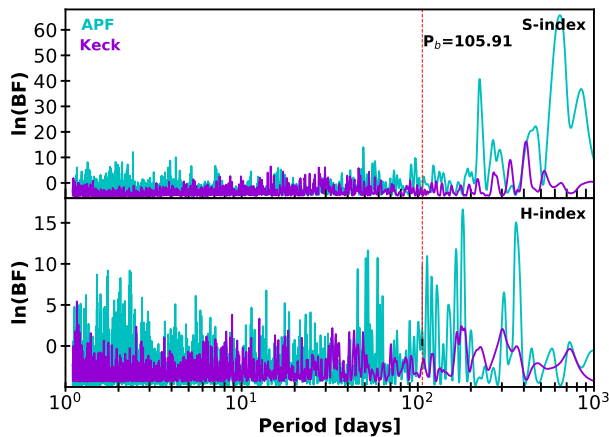


Figure 18. Top: Bayes factor periodogram of the S-index values of HD 180617 measured from the APF and Keck HIRES data sets in cyan and purple, respectively. There are no prominent peaks in the vicinity of the 105.91 day planet period. Bottom: Same as above, but for the H-index measurements extracted from the APF and Keck HIRES spectra, which also show a lack of peaks at the planet’s period.

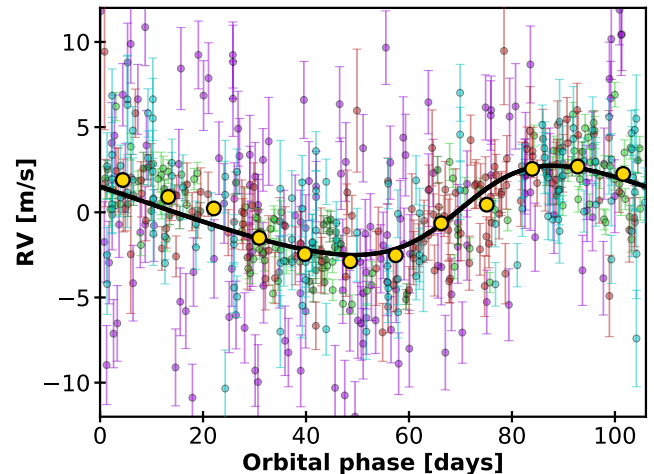


Figure 20. RV observations of HD 180617 phase folded to the best fit period of $P = 105.91$ days (colors match those in Figure 17). The error bars include the excess white noise “jitter” from our analysis, and the black solid curve denotes the maximum a posteriori Keplerian model. Yellow points depict the phase-binned RV data.

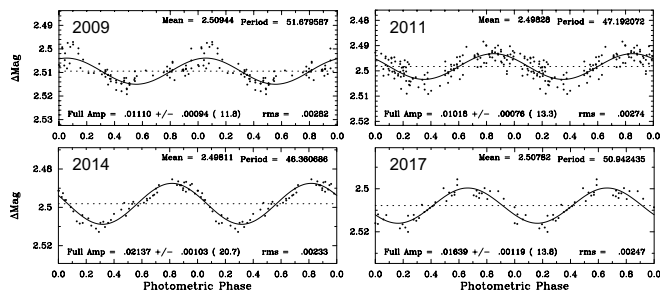


Figure 19. APT photometry for four of the nine seasons during which HD 180617 was observed. Combining the results across all nine seasons produces a weighted mean rotation period of 50.60 ± 0.41 days.

A total of 707 observations were obtained between 2009 through 2017 using the T10 0.8m APT at Fairborn Observatory (Figure 19). The comparison stars used in the photometric analysis were HD 183085 (an F2V star with $V = 6.72$, $B-V=0.36$) and HD 180945 (an F5V star with $V=7.15$ and $B-V=0.47$). We analyze each observing season for rotation and find periods for all nine seasons, with the star appearing to be “double spotted” in 2010 and 2015. In those two years, the rotation period is taken to be twice the observed photometric period. Combining the results across all nine seasons produces a weighted mean rotation period of 50.60 ± 0.41 days.

7.4. Orbital parameters

We find that the best orbital fit to the combined RV data set for HD 180617 is a mildly eccentric ($e = 0.101$), $P = 105.91$ day orbit with a semi-amplitude $K = 2.696$

ms^{-1} (Figure 20). This corresponds to a $12.214 M_{\oplus}$ mass planet in a 0.343 AU orbit around the host star, consistent with the findings of Kaminski et al. (2018). A search of the RV residuals periodogram does not reveal any evidence for additional signals.

8. DISCUSSION

In this study, we analyzed 34 Keck HIRES and 157 APF RV measurements of the K4V star HD 190007 along with 504 Keck HIRES and 300 APF RV measurements of the K0V star HD 216520. From these analyses we detect three new planets. Based on our derived orbital parameters, HD 190007 b and HD 216520 b are both close-in, sub-Neptune type planets while HD 216520 c is a longer period, temperate sub-Neptune planet. We also confirmed the orbital parameters of two previously published low-mass planets. First, we derived an updated orbital solution for the planet orbiting the M1.0V star GJ 686 reported by Affer et al. (2019) and Lalitha et al. (2019) using an additional 134 new RV APF measurements and 18 new PFS measurements. And second we updated the orbital solution of the planet orbiting the M3.0V star HD 180617 detailed in Kaminski et al. (2018), adding 126 new APF measurements to the combined data set.

8.1. Benefits of long baseline, multi-facility data sets

K- and M-dwarf stars make enticing radial velocity survey targets because 1) their lower stellar masses result in larger RV semi-amplitudes from an exoplanet with a set period and mass than would be induced on

hotter, more massive stellar types and 2) their lower effective temperatures result in a higher number of stellar absorption lines that increase the RV information content in their spectra (Beatty & Gaudi 2015). While, to our knowledge, HD 190007 and HD 216520 have only been included in the Keck HIRES and APF surveys described here, GJ 686 and HD 180617 have each been targeted by at least four independent surveys.

This array of data sets spanning long temporal baselines allows for the derivation of very precise orbital models for each of the planets and also for the comparison of both planetary and stellar variability detections between different instruments and facilities. Our final orbital and planetary parameters for each of the planets are summarized in Table 5. Each of the planetary $m \sin i$ values is determined to the $\sigma_K \geq 10$ level, a benefit of having many precise RV observations taken over extended baselines. When comparing to the confirmed planets listed on the Exoplanet Archive, less than a quarter (roughly 22%) of RV detected, sub-Neptune-mass planets have $m \sin i$ measured to this level. Planets with such precise $m \sin i$ values offer some of the best insights and constraints when modeling the formation, evolution, and dynamic interactions of planetary systems. Having such long baseline results that accurately constrain the stars' RV signal could also allow for the detection of N-body effects such as planet-planet scattering with more comprehensive modeling, similar to the use of transit timing variations in transit data.

We find that our final results for the previously published planets, GJ 686 b and HD 180617 b, are in good agreement with the earlier results found in Kaminski et al. (2018); Affer et al. (2019) and Lalitha et al. (2019). For both planets our derived planet periods, eccentricities, semi-amplitudes, and $m \sin i$ values are all within the $1\text{-}\sigma$ uncertainties across all three existing publications.

One particular strength of the APF telescope, with its ability to achieve nightly cadence on interesting RV target stars, is that the resulting data can help disentangle observational aliases. In particular, earlier versions of the HD 190007 data set showed strong signals at periods of both 11.72 and 1.09 days, which are daily aliases of one another. For example, earlier versions of the RV periodogram for HD 190007 showed an additional peak appeared at $P = 1.09$ days, corresponding to the 1 day alias ($f_{1.09d} = f_{11.72d} + f_{1day}$) of the 11.72 day signal. We had reason to suspect that the longer period signal was the true signature of the planet because the 1.09 day signal produced a notably lower $\ln(\text{BF}_5)$ value and required an orbital eccentricity of $e=0.119\pm 0.068$. This non-zero eccentricity seemed unlikely for a planet

on such a short period orbit, which we would expect to have circularized via tidal dissipation (Hadden & Lithwick 2017; Van Eylen & Albrecht 2015). But it was challenging to make a robust determination of which signal was caused by the planet and which was the alias. By observing the star for an additional season and ensuring that it underwent high cadence observations (Figure 1) we were able to update the analysis and found that the 1.09 day signal had dramatically decreased in significance, further strengthening our argument that the 11.72 day signal presented here is the true Keplerian signature of the planet. This same affect of being able to discern between true signals and observational aliases can be achieved by combining data from different facilities that have some degree of longitudinal spread across the globe. This enables a broader range of short-period observational cadences based on telescope separations and will help remove power from the 1 day alias that plagues single-site observations.

8.2. Potential for additional detection methods

Having discovered these planets via the radial velocity method, we investigate whether they might make good candidates for additional detection/characterization methods such as transit, astrometric, and direct imaging observations. We calculate transit probabilities using Winn (2010), and astrometric semi-amplitudes and maximum projected separations using Perryman (2011). We find that due to the combination of low mass and relatively short orbital periods, none of the five planets detailed in this work are expected to produce an astrometric semi-amplitude larger than 5 micro-arcseconds placing them all beyond the reach of Gaia's detection threshold. Similarly, the projected on-sky separation of the HD 190007, HD 216520, and HD 180617 planets from their host stars are all below 0.03 arcseconds, making them inaccessible to even the upcoming generation of Extremely Large Telescopes. GJ 686 b is a slightly more promising case, with a maximum projected separation of 0.058 arcsecond, but even this is on the very edge of performance expected from ground-based, thirty meter class facilities.

For the transit probability calculations, we need to make an assumption about the planets' sizes. We compare the minimum masses listed in Table 5 with the conditional distributions for a planet's radius given its mass presented in Figure 7 of Ning et al. (2018). We adopt a uniform radius assumption of $R = 3 R_{\oplus}$ for all of our planets as they correspond most closely to the Mass = $10 M_{\oplus}$ distribution. Inserting this radius assumption along with the planets' measured orbital parameters into

Table 5. Best fit orbital solution for each of the planets detailed above and the activity signals noted for HD 190007 and HD 216520. Reported values are the mean and standard deviation for each model parameter. Minimum mass and semi-major axis have been estimated by adopting the stellar masses listed for each star in Table 1

	HD 190007 Planet b	HD 190007 Activity	HD 216520 Planet b	HD 216520 Planet c	HD 216520 Activity	GL 686 Planet b	HD 180617 Planet b
P (days)	11.72±0.001	29.180±0.012	35.45±0.011	154.43±0.44	7767.35±1464.31	15.530±0.0011	105.911±0.109
K (m s^{-1})	5.64±0.55	3.54±0.90	2.28±0.20	1.29±0.22	1.90±0.35	3.004±0.180	2.696±0.224
e	0.14±0.07	0.31±0.15	0.09±0.06	0.12±0.08	0.19±0.12	0.050±0.030	0.101±0.053
ω (deg)	254.64±109.93	225±47	220.95±125.17	198.12±96.34	95.32±82.22	197.062±153.673	257.433±51.256
M_0 (deg)	100.78±92.27	214±47	48.72±9.69	48.72±9.69	113.61±9310.53	223.884±27.596	123.594±50.897
$\ln(BF_3)$	28.04	7.93	44.3	6.2	6.9	72.03	39.359
$\ln(BF_5)$	23.37	2.68	37.59	-0.52	0.18	65.88	33.062
$m \sin i$ (M_\oplus)	16.46±1.66	–	10.26±0.99	9.44 ± 1.63	–	6.624±0.432	12.214±1.05
a (AU)	0.092±0.0008	–	0.198±0.0004	0.528 ± 0.010	–	0.091±0.001	0.343±0.004

NOTE— M_0 values are referenced to the first RV epoch for each star, which can be found in Tables 6-9.

Equation 9 of Winn (2010) produces transit probabilities well below 1% for each of the planets.

While the radial velocity detections for all of these systems are robust we do not expect any of these planets to be particularly well-suited to additional methods of detection and characterization.

8.3. Comparison to close-in Kepler-multi planet systems

With minimum masses just at or below that of Neptune and periods in the 10-100 day range two of the planets discovered here (HD 190007 b and HD 216520 b) are reminiscent of the numerous super-Earth and sub-Neptune planets detected in transit by the *Kepler* mission (Figure 21). In particular, *Kepler* revealed that about half of stars in our galaxy harbor the small ($R_p \leq 4R_\oplus$), close-in ($P \leq 100$ days) planets, which are often found in tightly-spaced, multi-planet systems (Lissauer et al. 2011; Latham et al. 2011; Lissauer et al. 2014; Rowe et al. 2014). Most surprisingly, the multiple planets in the same systems tend to be similar in both mass and radius (Millholland et al. 2017; Wang 2017; Weiss et al. 2018).

That is, statistically speaking, for a given short-period super-Earth or sub-Neptune planet such as HD 190007 b or HD 216520 b we would expect the existence of additional close-in planets and for those planets to have masses similar (within a factor of two) to that of the detected planet. While HD216520 c is very similar in mass to HD216520 b, much like the multi-planet systems found with *Kepler*, it does not have an orbital period within a factor of two of the inner planet as would be expected for a *Kepler* multi-planet system. We

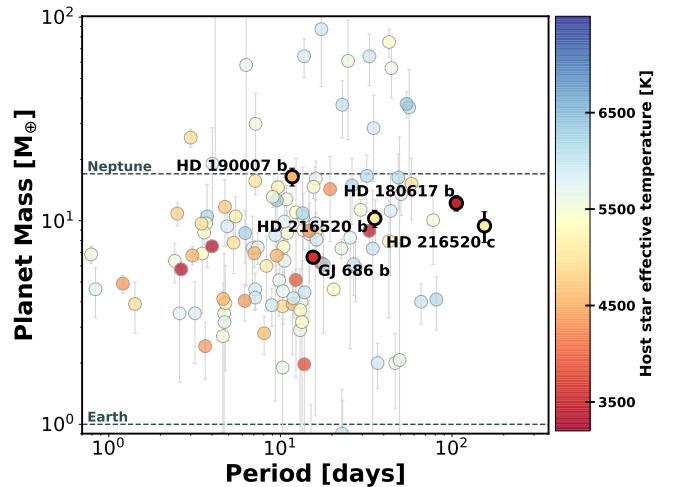


Figure 21. Out of the 136 *Kepler* and *K2* sub-Neptune mass exoplanets that have orbital periods less than 100 days, 116 (85%) are in multi-planet systems. Our two new and two updated planets, labeled here in black, land in a very similar region of period-mass parameter space as the *Kepler* multi-planet systems. If the planets in this paper were formed in a similar manner as the ones found by *Kepler*, this would suggest that additional, close-in and similar mass planets may be present in those systems. Note that our the new planets have only minimum mass measurements, as their inclination is unknown, and so their positions on this plot are lower limits.

therefore examine the possibility that there may be additional planets with periods less than 100 days orbiting HD 190007 and HD 216520. Neither star’s data set shows evidence of additional, significant signals in their respective RV residuals periodogram (Figures 1 and 6). Yet this does not rule out the possibility that additional

signals might be present at significance levels obscured by effects from stellar activity, our observing cadence, and our RV precision, among others. To test our data sets’ ability to detect such signals we perform an injection and recovery test using the same residual RVs used to create those periodograms. First, we define period and semi-amplitude ranges similar to those of the small, close-in planets detected by *Kepler*: $0.5 < P < 300$ days and $0.5 < K < 10 \text{ m s}^{-1}$. We then randomly draw a period and semi-amplitude value from a log distribution bounded by these end points and inject the corresponding Keplerian signal into the RV residuals. We generate a Lomb-Scargle periodogram of the resulting RVs and calculate the False Alarm Probability (FAP) of the periodogram at the highest peak within 10% of the injected period. We define our recovery criteria such that cases when the resulting FAP value is below 0.01 are considered to be successful detections of the planet. We execute this process 100,000 times for each star’s residuals data sets and visualize the results in Figure 22. The cool colored regions of the plot (FAP < 0.01) represent period and semi-amplitude combinations that we successfully recover. We note here that this process is an estimate of our ability to detect a periodic signal with a certain period. This is not the estimate of our probability of recovering a Keplerian signal. Finding a periodic signal is a step in that process, so our detection probabilities are likely over-estimates of our ability to actually recover and characterize a planet’s orbit.

In the case of HD 190007, for which we have 123 RV epochs taken over two decades, we are sensitive to planets with semi-amplitudes down to $\sim 3 \text{ m s}^{-1}$ for periods out to one year. Given the star’s mass, the 3 m s^{-1} sensitivity level corresponds to planets in the 4-28 M_{\oplus} range. As HD 190007 b has an $m \sin i$ value of 16.46 M_{\oplus} we are most interested in our ability to detect “similar” planets like those we’d expect to see in a *Kepler* -like system, which would fall in the 8-30 M_{\oplus} mass range. While planets with masses $\geq 20 M_{\oplus}$ should be detectable throughout the 1-100 day period range populated by the close-in *Kepler* multi-planet systems, those in the 8-20 M_{\oplus} range could be obscured at periods longer than 10 days.

For HD 216520, with its 369 RV epochs taken over nineteen years, the injection/recovery process suggests that we are sensitive to planets with semi-amplitudes down to $\sim 1 \text{ m s}^{-1}$ for periods out to 300 days. A 1 m s^{-1} signal in the HD 216520 data set corresponds to a planet with mass ranging from 1.5-10 M_{\oplus} when considering periods less than 300 days. Given the 11.63 M_{\oplus} $m \sin i$ value of HD 216520 b, and again assuming that *Kepler* -like systems will have planets of similar masses,

we would expect any additional planets in the system to have masses in the 5-20 M_{\oplus} range, making it likely that we would have noticed their presence in our existing data.

Similar to our solar system, the *Kepler* multi-planet systems tend to be well organized - they have small mutual inclinations, circular orbits, and are generally well aligned with the host star’s rotation. Since both HD 190007 b and HD 216520 b are on circular orbits, additional co-planar planets within these systems should be able to survive on similarly circular orbits beyond the Hill stability threshold. But as seen above, we rule out the presence of additional, close-in planets with masses similar to our newly detected planets in tightly-spaced stable orbits.

One possibility is that because radial velocity detections measure a planet’s minimum mass, and not its true mass, then one or both of these planets may actually be a more massive, gas giant on a highly inclined orbit. Gas giants are significantly less likely to be accompanied by either other close-in planets (Steffen et al. 2012; Cañas et al. 2019), or planets with similar masses (Wang 2017). HD 216520 in particular has an extremely small reported $v \sin i$ ($0.2 \pm 0.05 \text{ km s}^{-1}$) compared with stars that have similar T_{eff} (5082 K) lending some credence to the idea that the planet’s orbital plane is far from the line of sight. As the orbits of most small planets align with their host star’s equator (Winn & Fabrycky 2015; Wang et al. 2018), HD 216520’s small $v \sin i$ value suggests that the planet is likely to be a highly inclined gas giant, otherwise the projected RV is too small to be detected. But while we selected the Brewer et al. (2016) $v \sin i$ value for consistency with the other stellar parameters reported in Table 1 there are two additional $v \sin i$ measurements for this star in the literature. Luck (2017) reports a $v \sin i$ value of 2.5 km s^{-1} while Mishenina et al. (2008) finds $v \sin i = 1.4 \text{ km s}^{-1}$. If one of these larger values is a more accurate measurement of the HD 216520’s rotational velocity, which seems reasonable given the star’s T_{eff} , then it would be less likely that HD 216520 b is a gas giant masquerading as a Neptune.

An alternate explanation is that the planets detected in this paper using the RV technique and the planets detected by *Kepler* are not from the same population, and therefore do not share similar observational properties. There is an unsolved discrepancy of hot-Jupiters occurrence rate between the *Kepler* and RV samples, which is partially attributed to the fact that the *Kepler* sample has lower metallicity than the RV sample (Guo et al. 2017) as the RV technique performs better on high-metallicity stars because of the increased information content in their stellar spectra. As pointed

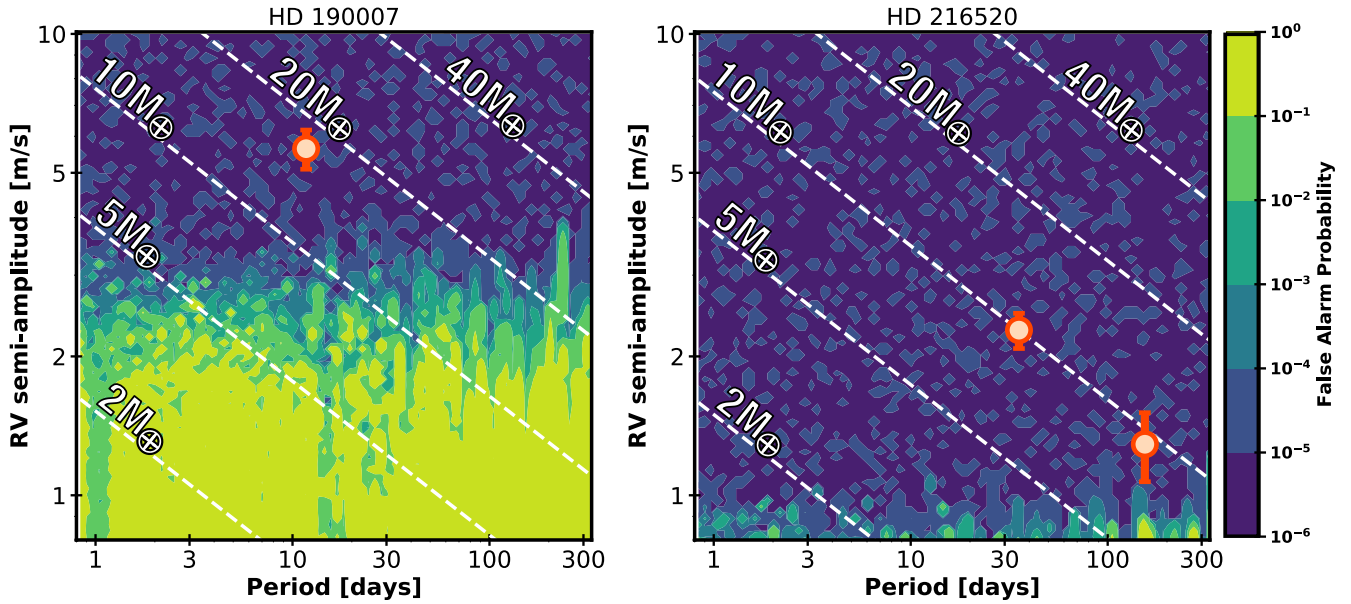


Figure 22. Injection and recovery contour maps for HD 190007 (left) and HD 216520 (right), with the newly discovered planets shown as orange circles. Coloration represents the FAP value of the LS periodogram at the injected period, with the darker colors (FAP < 0.01) representing planets that were successfully recovered. White lines show the RV semi-amplitude of a given planet mass as a function of period. For HD 190007 we are sensitive to planets with masses greater than 5-20 M_{\oplus} depending on the period, while for HD 216520 we are sensitive to planets with masses greater than 1-10 M_{\oplus} . The lack of a discovery of similar mass and period planets in these systems is in marked contrast with *Kepler* discoveries where $\sim 85\%$ of planets have neighbors that are close in mass, radius, and period.

out by Brewer et al. (2018), super-Earth/sub-Neptune’s multiplicity is anti-correlated with host stellar metallicity. Metal-rich stars, HD 190007 for example ($[\text{Fe}/\text{H}] = 0.16 \pm 0.05$), are less likely to host multiple planet systems. This raises the interesting possibility that our two new planets detected here have followed a different path of planet formation than that taken by the majority of *Kepler* planets. Though our work has a small sample size, the addition of even a small number of planets helps to point the way towards a future verification or rebuttal of this picture.

©2020

The research was carried out in part at the Jet Propulsion Laboratory, California Institute of Technology, under a contract with the National Aeronautics and Space Administration (80NM0018D0004).

The work herein is based on observations obtained at the W. M. Keck Observatory, which is operated jointly by the University of California and the California Institute of Technology, and we thank the UC-Keck and NASA-Keck Time Assignment Committees for their support. We also wish to extend our special thanks to those of Hawaiian ancestry on whose sacred mountain of Mauna Kea we are privileged to be guests. Without their generous hospitality, the Keck observations presented herein would not have been possible. The work

herein is also based on observations obtained with the Automated Planet Finder (APF) telescope and its Levy Spectrometer at Lick Observatory, along with data gathered with the 6.5 meter Magellan Telescopes located at Las Campanas Observatory, Chile. G.W.H. acknowledges long-term support from NASA, NSF, Tennessee State University, and the State of Tennessee through its Centers of Excellence program.

This research has made use of the Keck Observatory Archive (KOA), which is operated by the W. M. Keck Observatory and the NASA Exoplanet Science Institute (NExSci), under contract with the National Aeronautics and Space Administration. We specifically acknowledge the 83 RVs used in the analysis of HD 216520 that are based on spectra taken by the California Planet Search team and archived in the Keck Observatory Archive. This research has made use of the SIMBAD database, operated at CDS, Strasbourg, France.

This publication makes use of VOSA, developed under the Spanish Virtual Observatory project supported by the Spanish MINECO through grant AyA2017-84089. VOSA has been partially updated by using funding from the European Union’s Horizon 2020 Research and Innovation Programme, under Grant Agreement n^o 776403 (EXOPLANETS-A)

Simulations in this paper made use of the REBOUND code which is freely available at <http://github.com/hannorein/rebound>.

Facilities: UCO/Lick: The APF (Levy spectrograph), Magellan: Clay (Planet Finder Spectrograph), Keck I: (HIRES), TSU:AST (T4 and T12 APTs)

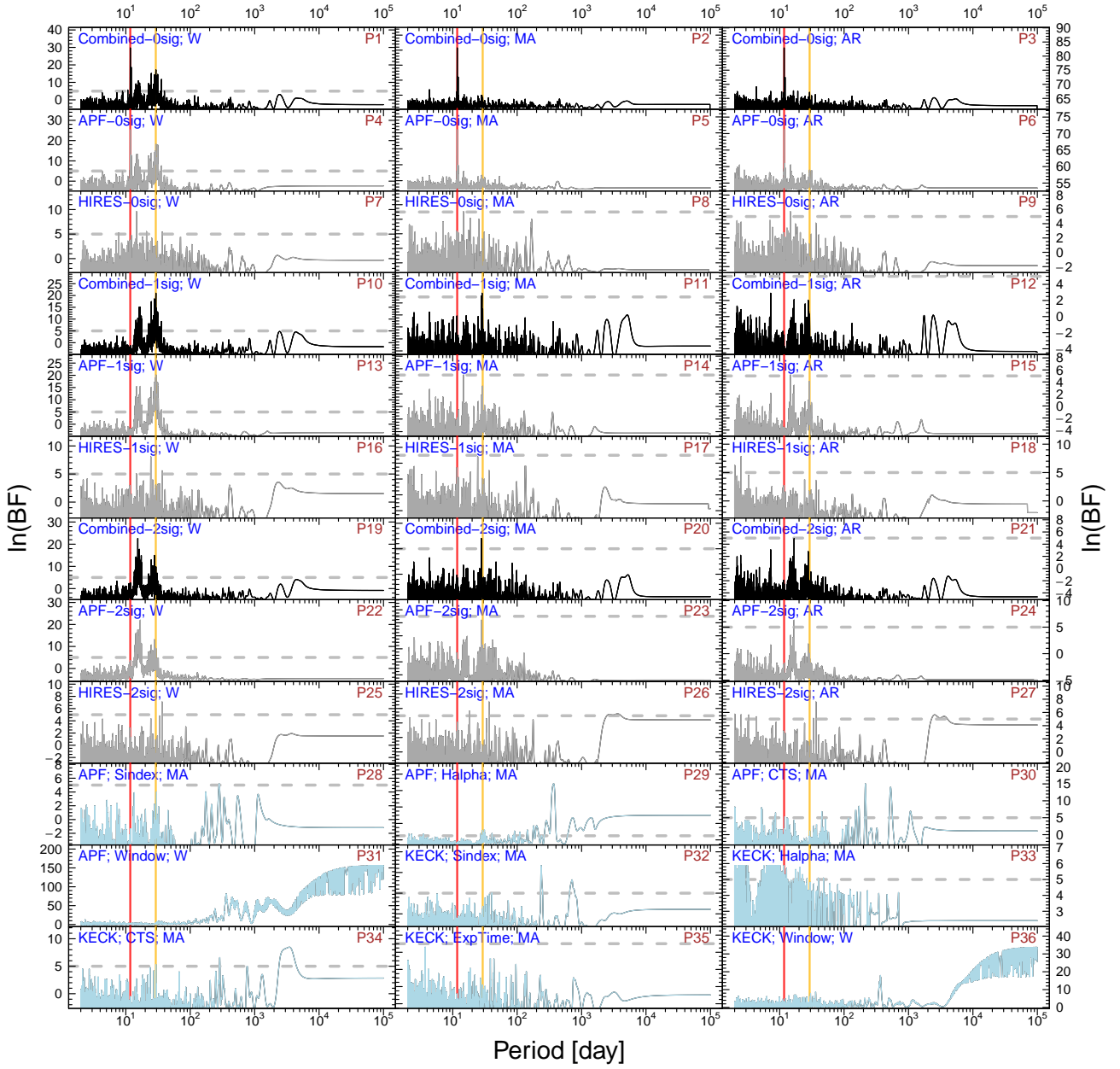


Figure 23. Full set of Bayes Factor Periodograms for HD 190007. The red line denotes the 11.72 day signal that we take to be the true planet signal, while the gold line shows the 29 day period that we find to be caused by stellar variability.

APPENDIX

A. BAYES FACTOR PERIODOGRAMS

Figures 23, 24, 25, and 26 depict the full set of Bayes Factor Periodograms for each of the four stars included in this study.

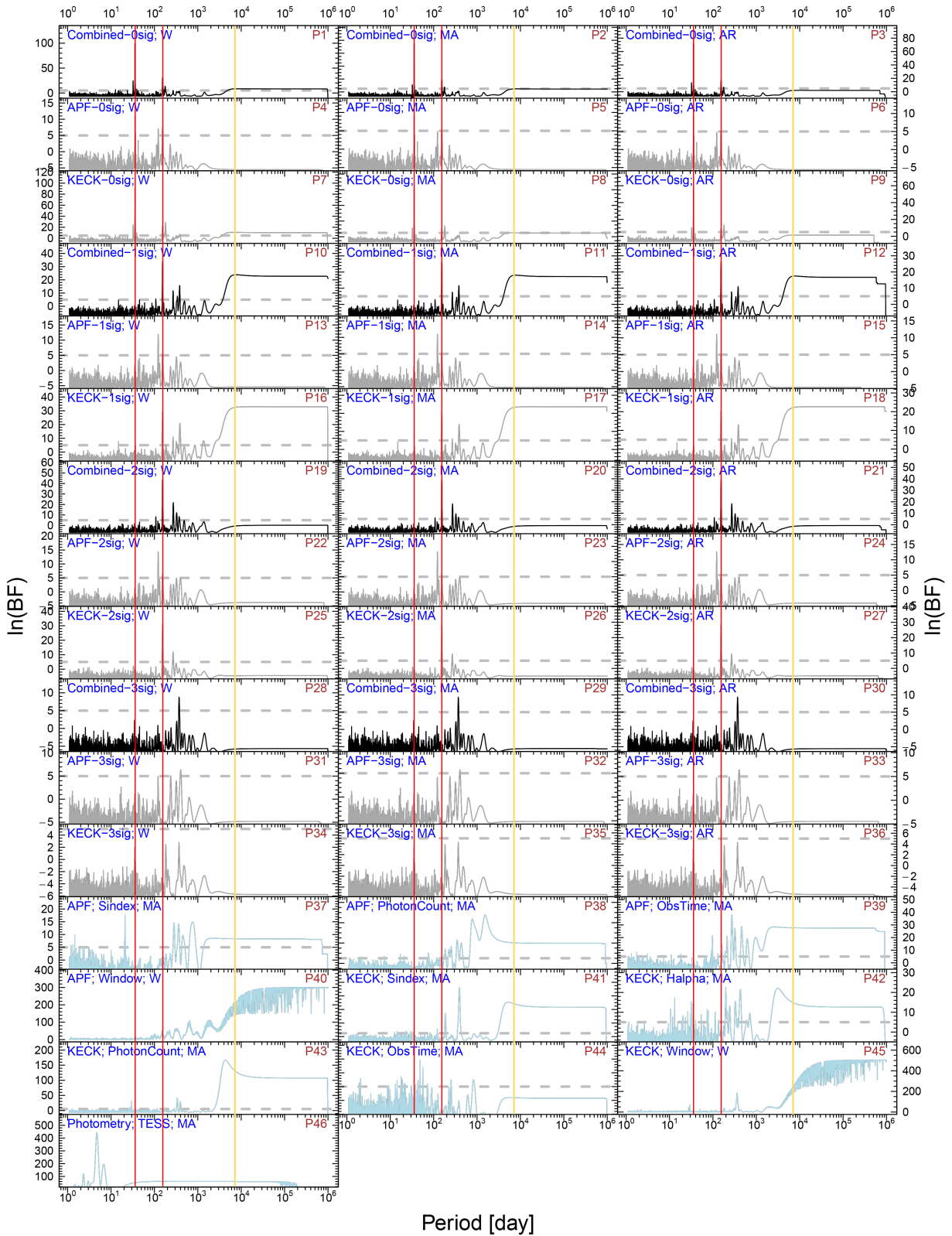


Figure 24. Full set of Bayes Factor Periodograms for HD 216520. The red lines denote the 35.45 and 154.43 day signals that we take to be planets. The gold line shows the additional 7767.35 day signal that we believe to be caused by the star’s magnetic activity cycle.

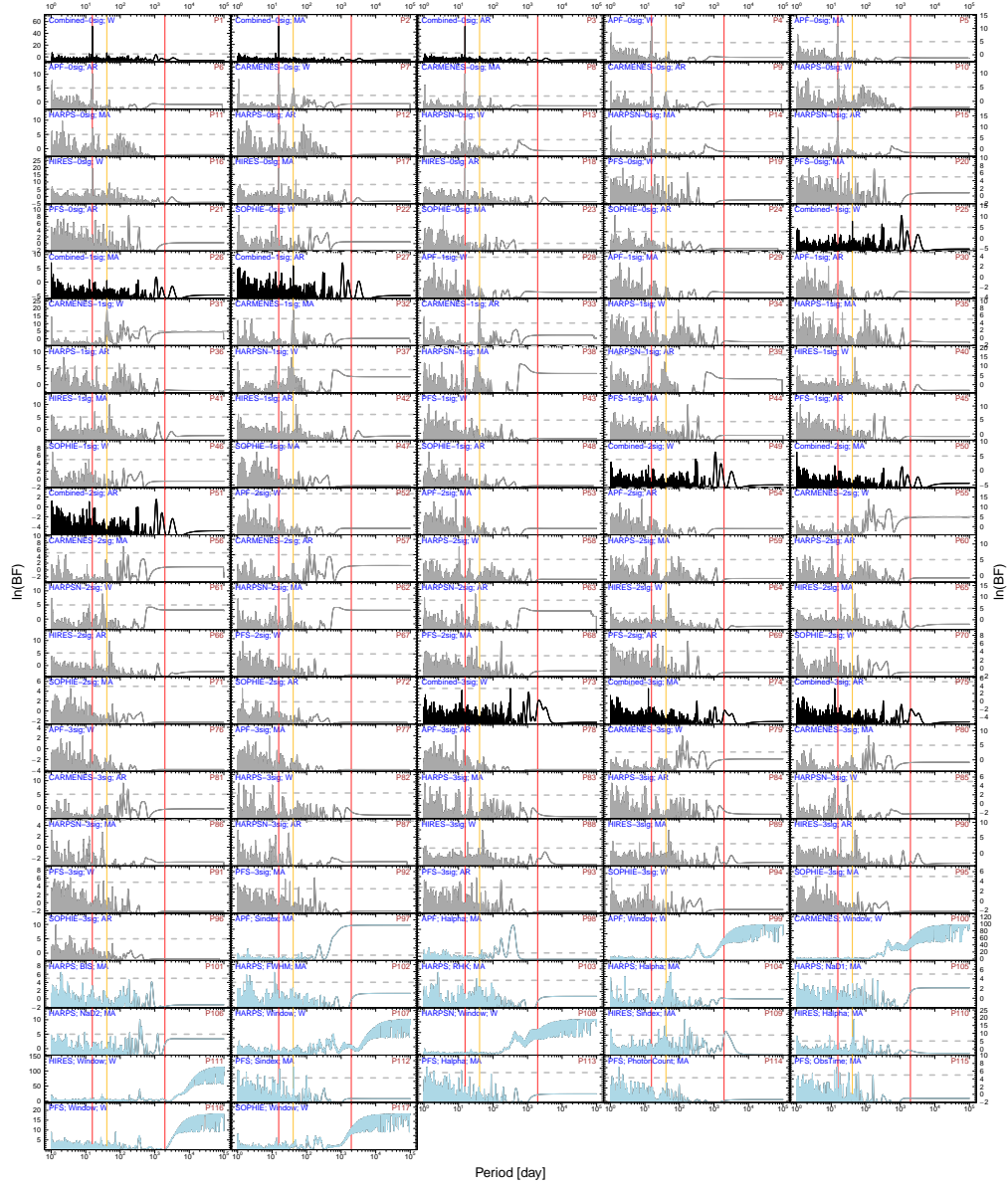


Figure 25. Full set of Bayes Factor Periodograms for GL 686. The red line denotes the 15d planet signal originally identified in *Affer et al. (2019)* and *Lalitha et al. (2019)* and confirmed again in this work. The gold lines show the ~ 40 day and $\sim 2,000$ day signals that we identify as the star’s rotational and magnetic activity cycles, respectively.

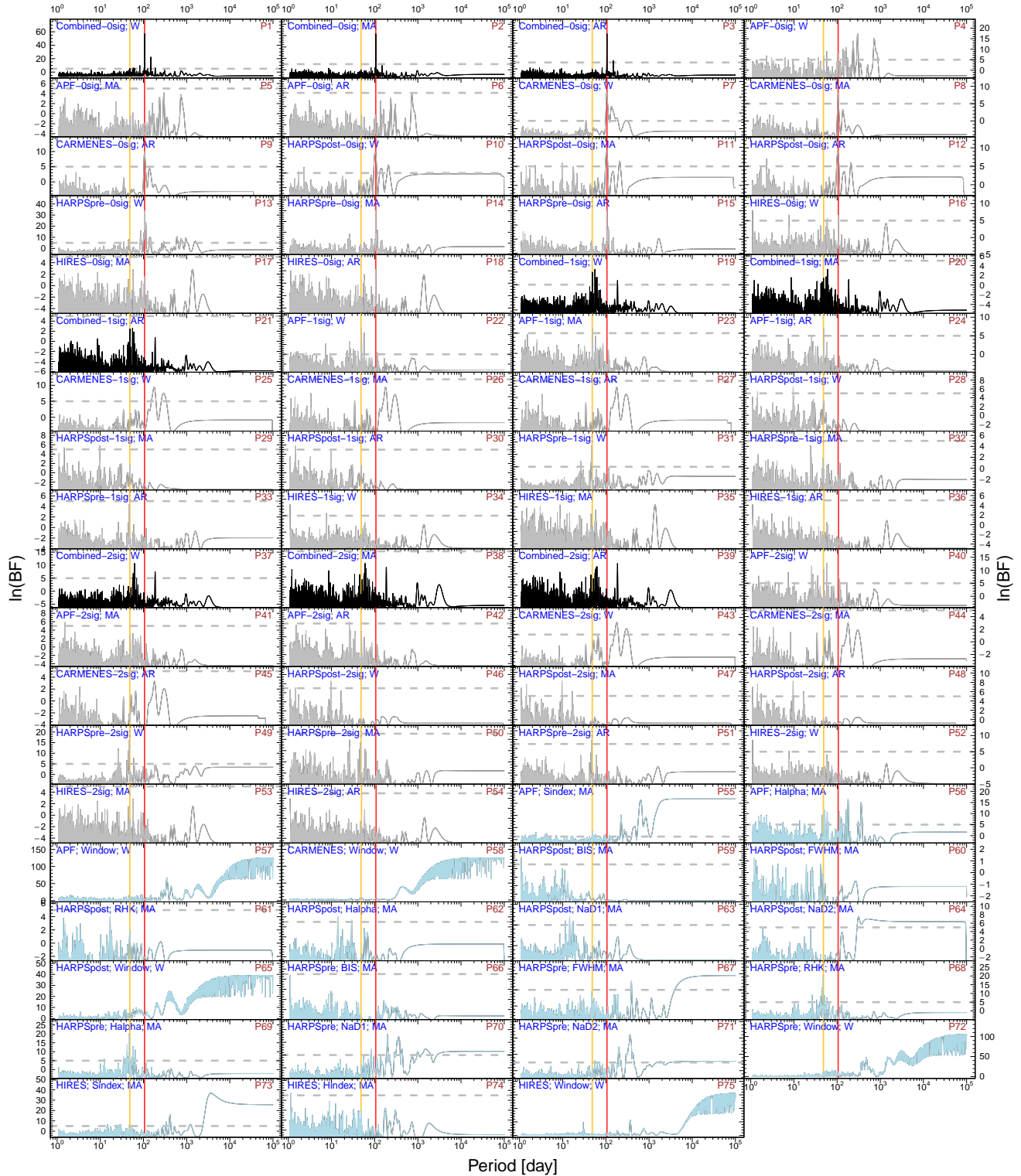


Figure 26. Full set of Bayes Factor Periodograms for HD 180617. The red line denotes the 105.91 day planet signal originally identified in Kaminski et al. (2018) and confirmed in this work. The gold line shows the ~ 50 day activity signal seen in the HARPS H- α measurements and the APT photometry that we take to be the star’s rotation period.

B. RADIAL VELOCITY MEASUREMENTS

Tables 6-9 contain the new RVs from HIRES, the APF, PFS, and HARPS TERRA presented in this paper. A portion of each table is shown here for guidance regarding their forms and content, while the full tables are published in the machine-readable format.

Table 6. New Radial Velocity data for HD 190007

MJD	RV [m s ⁻¹]	σ_{RV} [m s ⁻¹]	S-index	H-index	Instrument
2450984.05436	7.41	1.33	0.7281	-1	HIRES
2451013.94476	-1.73	1.46	0.6926	-1	HIRES
2451050.86802	-6.75	1.35	0.7218	-1	HIRES
2451069.88122	-1.29	1.47	0.7261	-1	HIRES
2451075.80608	7.09	1.21	0.6631	-1	HIRES
2451341.05512	-7.35	1.52	0.6168	-1	HIRES
2451368.86865	-5.04	1.57	0.5584	-1	HIRES
2451409.92287	2.89	1.99	0.6589	-1	HIRES
2451439.81141	3.88	1.54	0.6635	-1	HIRES
2451439.81802	7.60	1.60	0.6523	-1	HIRES

Table 7. New Radial Velocity data for HD 216520

MJD	RV [m s ⁻¹]	σ_{RV} [m s ⁻¹]	S-index	H-index	Instrument
2452188.92575	-2.46	1.25	0.1696	-1	HIRES
2452189.85472	-0.41	1.49	0.185	-1	HIRES
2452235.68115	-1.11	1.38	0.1799	-1	HIRES
2452446.08978	1.34	1.37	0.1814	-1	HIRES
2452487.04685	-1.40	1.31	0.1802	-1	HIRES
2452487.93822	-3.99	1.32	0.171	-1	HIRES
2452488.96981	-2.27	1.25	0.1678	-1	HIRES
2452537.89594	-2.53	1.38	0.1747	-1	HIRES
2452574.81330	0.48	1.47	0.1363	-1	HIRES
2452833.03093	3.99	1.57	0.1383	-1	HIRES

Table 8. New Radial Velocity data for GJ 686

MJD	RV [m s ⁻¹]	σ_{RV} [m s ⁻¹]	S-index	H-index	Instrument
2453159.74925	3.65	0.95	0.54270	0.28195	TERRA
2453574.62254	0.81	0.82	0.67370	0.28953	TERRA
2453817.86816	-0.83	0.75	0.63931	0.29228	TERRA
2454174.87133	-1.72	0.77	0.63735	0.26124	TERRA
2454194.90763	2.51	0.78	0.73922	0.28956	TERRA
2454300.64483	-2.47	0.72	0.65581	0.28934	TERRA
2454948.86154	-1.17	0.57	0.66352	0.23889	TERRA
2454950.86206	-2.71	0.64	0.65440	0.23478	TERRA
2454956.83071	-0.53	0.88	0.56384	0.23619	TERRA
2455390.64094	1.13	1.10	0.67622	0.27807	TERRA

Table 9. New Radial Velocity data for HD 180617

MJD	RV [m s ⁻¹]	σ_{RV} [m s ⁻¹]	S-index	H-index	Instrument
2453159.81073	-1.89	0.68	0.93516	0.24810	TERRA
2453517.83909	1.13	0.67	1.08339	0.21657	TERRA
2453572.76530	1.38	1.52	1.15631	0.11502	TERRA
2453573.72190	-1.81	0.64	1.07858	0.19700	TERRA
2453574.68500	-1.82	0.41	1.11689	0.16847	TERRA
2453575.65016	-1.55	0.29	1.01041	0.21838	TERRA
2453576.65304	-2.48	0.75	1.00409	0.21559	TERRA
2453577.67857	-0.95	0.47	1.06946	0.19882	TERRA
2453578.67547	-1.44	0.37	0.99462	0.22405	TERRA
2453579.65731	-2.24	0.45	0.98758	0.23099	TERRA

REFERENCES

- 1997, ESA Special Publication, Vol. 1200, The HIPPARCOS and TYCHO catalogues. Astrometric and photometric star catalogues derived from the ESA HIPPARCOS Space Astrometry Mission
- Affer, L., Damasso, M., Micela, G., et al. 2019, *A&A*, 622, A193, doi: [10.1051/0004-6361/201834868](https://doi.org/10.1051/0004-6361/201834868)
- Aguilera-Gómez, C., Ramírez, I., & Chanamé, J. 2018, *A&A*, 614, A55, doi: [10.1051/0004-6361/201732209](https://doi.org/10.1051/0004-6361/201732209)
- Anders, F., Khalatyan, A., Chiappini, C., et al. 2019, *A&A*, 628, A94, doi: [10.1051/0004-6361/201935765](https://doi.org/10.1051/0004-6361/201935765)
- Anglada-Escudé, G., & Butler, R. P. 2012, *ApJS*, 200, 15, doi: [10.1088/0067-0049/200/2/15](https://doi.org/10.1088/0067-0049/200/2/15)
- Bai, Y., Liu, J., Bai, Z., Wang, S., & Fan, D. 2019, *AJ*, 158, 93, doi: [10.3847/1538-3881/ab3048](https://doi.org/10.3847/1538-3881/ab3048)
- Baranne, A., Queloz, D., Mayor, M., et al. 1996, *A&AS*, 119, 373
- Bayo, A., Rodrigo, C., Barrado Y Navascués, D., et al. 2008, *A&A*, 492, 277, doi: [10.1051/0004-6361/200810395](https://doi.org/10.1051/0004-6361/200810395)
- Beatty, T. G., & Gaudi, B. S. 2015, *PASP*, 127, 1240, doi: [10.1086/684264](https://doi.org/10.1086/684264)
- Bensby, T., Feltzing, S., & Oey, M. S. 2014, *A&A*, 562, A71, doi: [10.1051/0004-6361/201322631](https://doi.org/10.1051/0004-6361/201322631)
- Bermejo, J. M., Asensio Ramos, A., & Allende Prieto, C. 2013, *VizieR Online Data Catalog*, J/A+A/553/A95
- Bianchi, L., Shiao, B., & Thilker, D. 2017, *ApJS*, 230, 24, doi: [10.3847/1538-4365/aa7053](https://doi.org/10.3847/1538-4365/aa7053)
- Biazzo, K., Frasca, A., Catalano, S., & Marilli, E. 2007, *Astronomische Nachrichten*, 328, 938, doi: [10.1002/asna.200710781](https://doi.org/10.1002/asna.200710781)
- Bland-Hawthorn, J., & Gerhard, O. 2016, *ARA&A*, 54, 529, doi: [10.1146/annurev-astro-081915-023441](https://doi.org/10.1146/annurev-astro-081915-023441)
- Boeche, C., & Grebel, E. K. 2016, *A&A*, 587, A2, doi: [10.1051/0004-6361/201526758](https://doi.org/10.1051/0004-6361/201526758)
- Bopp, B. W., & Espenak, F. 1977, *AJ*, 82, 916, doi: [10.1086/112146](https://doi.org/10.1086/112146)
- Bouchy, F., Pepe, F., & Queloz, D. 2001, *Astronomy & Astrophysics*, 374, 733, doi: [10.1051/0004-6361:20010730](https://doi.org/10.1051/0004-6361:20010730)
- Bouchy, F., Hébrard, G., Delfosse, X., et al. 2011, in *EPSC-DPS Joint Meeting 2011*, Vol. 2011, 240
- Bourges, L., Mella, G., Lafrasse, S., et al. 2017, *VizieR Online Data Catalog*, II/346
- Bovy, J. 2016, *ApJ*, 817, 49, doi: [10.3847/0004-637X/817/1/49](https://doi.org/10.3847/0004-637X/817/1/49)
- Brandt, T. D., & Huang, C. X. 2015, *ApJ*, 807, 24, doi: [10.1088/0004-637X/807/1/24](https://doi.org/10.1088/0004-637X/807/1/24)
- Brewer, J. M., Fischer, D. A., Valenti, J. A., & Piskunov, N. 2016, *ApJS*, 225, 32, doi: [10.3847/0067-0049/225/2/32](https://doi.org/10.3847/0067-0049/225/2/32)
- Brewer, J. M., Wang, S., Fischer, D. A., & Foreman-Mackey, D. 2018, *ApJL*, 867, L3, doi: [10.3847/2041-8213/aae710](https://doi.org/10.3847/2041-8213/aae710)
- Bryan, M. L., Knutson, H. A., Lee, E. J., et al. 2019, *AJ*, 157, 52, doi: [10.3847/1538-3881/aaf57f](https://doi.org/10.3847/1538-3881/aaf57f)
- Buchhave, L. A., Dressing, C. D., Dumusque, X., et al. 2016, *AJ*, 152, 160, doi: [10.3847/0004-6256/152/6/160](https://doi.org/10.3847/0004-6256/152/6/160)
- Burt, J., Holden, B., Hanson, R., et al. 2015, *Journal of Astronomical Telescopes, Instruments, and Systems*
- Burt, J. A., Nielsen, L. D., Quinn, S. N., et al. 2020, *AJ*, 160, 153, doi: [10.3847/1538-3881/abac0c](https://doi.org/10.3847/1538-3881/abac0c)
- Butler, R. P., Marcy, G. W., Williams, E., et al. 1996, *PASP*, 108, 500, doi: [10.1086/133755](https://doi.org/10.1086/133755)
- Butler, R. P., Vogt, S. S., Laughlin, G., et al. 2017, *AJ*, 153, 208, doi: [10.3847/1538-3881/aa66ca](https://doi.org/10.3847/1538-3881/aa66ca)
- Cañas, C. I., Wang, S., Mahadevan, S., et al. 2019, *ApJL*, 870, L17, doi: [10.3847/2041-8213/aafale](https://doi.org/10.3847/2041-8213/aafale)
- Casagrande, L., Portinari, L., & Flynn, C. 2006, *MNRAS*, 373, 13, doi: [10.1111/j.1365-2966.2006.10999.x](https://doi.org/10.1111/j.1365-2966.2006.10999.x)

- Casagrande, L., Ramírez, I., Meléndez, J., Bessell, M., & Asplund, M. 2010, *A&A*, 512, A54, doi: [10.1051/0004-6361/200913204](https://doi.org/10.1051/0004-6361/200913204)
- Chambers, J. E., Wetherill, G. W., & Boss, A. P. 1996, *Icarus*, 119, 261, doi: [10.1006/icar.1996.0019](https://doi.org/10.1006/icar.1996.0019)
- Chelli, A., Duvert, G., Bourguès, L., et al. 2016, *A&A*, 589, A112, doi: [10.1051/0004-6361/201527484](https://doi.org/10.1051/0004-6361/201527484)
- Chen, Y., Girardi, L., Bressan, A., et al. 2014, *MNRAS*, 444, 2525, doi: [10.1093/mnras/stu1605](https://doi.org/10.1093/mnras/stu1605)
- Christiansen, J. L., Vanderburg, A., Burt, J., et al. 2017, *AJ*, 154, 122, doi: [10.3847/1538-3881/aa832d](https://doi.org/10.3847/1538-3881/aa832d)
- Cosentino, R., Lovis, C., Pepe, F., et al. 2012, in *Society of Photo-Optical Instrumentation Engineers (SPIE) Conference Series*, Vol. 8446, *Society of Photo-Optical Instrumentation Engineers (SPIE) Conference Series*, 1
- Crane, J. 2010, in *Astronomy of Exoplanets with Precise Radial Velocities*, 19
- Crane, J. D., Shectman, S. A., & Butler, R. P. 2006, *Society of Photo-Optical Instrumentation Engineers (SPIE) Conference Series*, Vol. 6269, *The Carnegie Planet Finder Spectrograph*, 626931
- Crane, J. D., Shectman, S. A., Butler, R. P., Thompson, I. B., & Burley, G. S. 2008, *Society of Photo-Optical Instrumentation Engineers (SPIE) Conference Series*, Vol. 7014, *The Carnegie Planet Finder Spectrograph: a status report*, 701479
- Cummings, J. D., Deliyannis, C. P., Maderak, R. M., & Steinhauer, A. 2017, *AJ*, 153, 128, doi: [10.3847/1538-3881/aa5b86](https://doi.org/10.3847/1538-3881/aa5b86)
- Curtis, J. L., Agüeros, M. A., Douglas, S. T., & Meibom, S. 2019, *ApJ*, 879, 49, doi: [10.3847/1538-4357/ab2393](https://doi.org/10.3847/1538-4357/ab2393)
- Cutri, R. M., & et al. 2012, *VizieR Online Data Catalog*, II/311
- Cutri, R. M., Skrutskie, M. F., van Dyk, S., et al. 2003, *VizieR Online Data Catalog*, 2246
- Dawson, R. I., & Fabrycky, D. C. 2010, *ApJ*, 722, 937, doi: [10.1088/0004-637X/722/1/937](https://doi.org/10.1088/0004-637X/722/1/937)
- Díaz, M. R., Jenkins, J. S., Tuomi, M., et al. 2018, *AJ*, 155, 126, doi: [10.3847/1538-3881/aaa896](https://doi.org/10.3847/1538-3881/aaa896)
- Dumusque, X., Borsa, F., Damasso, M., et al. 2017, *A&A*, 598, A133, doi: [10.1051/0004-6361/201628671](https://doi.org/10.1051/0004-6361/201628671)
- Duncan, D. K., Vaughan, A. H., Wilson, O. C., et al. 1991, *ApJS*, 76, 383, doi: [10.1086/191572](https://doi.org/10.1086/191572)
- Dutra-Ferreira, L., Pasquini, L., Smiljanic, R., Porto de Mello, G. F., & Steffen, M. 2016, *A&A*, 585, A75, doi: [10.1051/0004-6361/201526783](https://doi.org/10.1051/0004-6361/201526783)
- Egeland, R. 2018, *ApJS*, 236, 19, doi: [10.3847/1538-4365/aab771](https://doi.org/10.3847/1538-4365/aab771)
- Eker, Z., Bakış, V., Bilir, S., et al. 2018, *MNRAS*, 479, 5491, doi: [10.1093/mnras/sty1834](https://doi.org/10.1093/mnras/sty1834)
- Feng, F., Tuomi, M., & Jones, H. R. A. 2017a, *A&A*, 605, A103, doi: [10.1051/0004-6361/201730406](https://doi.org/10.1051/0004-6361/201730406)
- . 2017b, *MNRAS*, 470, 4794, doi: [10.1093/mnras/stx1126](https://doi.org/10.1093/mnras/stx1126)
- Feng, F., Tuomi, M., Jones, H. R. A., Butler, R. P., & Vogt, S. 2016, *MNRAS*, 461, 2440, doi: [10.1093/mnras/stw1478](https://doi.org/10.1093/mnras/stw1478)
- Feng, F., Crane, J. D., Xuesong Wang, S., et al. 2019, *ApJS*, 242, 25, doi: [10.3847/1538-4365/ab1b16](https://doi.org/10.3847/1538-4365/ab1b16)
- Franchini, M., Morossi, C., di Marcantonio, P., Malagnini, M. L., & Chavez, M. 2014, *MNRAS*, 442, 220, doi: [10.1093/mnras/stu873](https://doi.org/10.1093/mnras/stu873)
- Frasca, A., Biazzo, K., Lanzafame, A. C., et al. 2015, *A&A*, 575, A4, doi: [10.1051/0004-6361/201424409](https://doi.org/10.1051/0004-6361/201424409)
- Gagné, J., Mamajek, E. E., Malo, L., et al. 2018, *ApJ*, 856, 23, doi: [10.3847/1538-4357/aaae09](https://doi.org/10.3847/1538-4357/aaae09)
- Gaia Collaboration, Brown, A. G. A., Vallenari, A., et al. 2016, *A&A*, 595, A2, doi: [10.1051/0004-6361/201629512](https://doi.org/10.1051/0004-6361/201629512)
- . 2018, *A&A*, 616, A1, doi: [10.1051/0004-6361/201833051](https://doi.org/10.1051/0004-6361/201833051)
- Gladman, B. 1993, *Icarus*, 106, 247, doi: [10.1006/icar.1993.1169](https://doi.org/10.1006/icar.1993.1169)
- Gomes da Silva, J., Santos, N. C., Bonfils, X., et al. 2011, *A&A*, 534, A30, doi: [10.1051/0004-6361/201116971](https://doi.org/10.1051/0004-6361/201116971)
- . 2012, *A&A*, 541, A9, doi: [10.1051/0004-6361/201118598](https://doi.org/10.1051/0004-6361/201118598)
- González Hernández, J. I., & Bonifacio, P. 2009, *A&A*, 497, 497, doi: [10.1051/0004-6361/200810904](https://doi.org/10.1051/0004-6361/200810904)
- Gossage, S., Conroy, C., Dotter, A., et al. 2018, *ApJ*, 863, 67, doi: [10.3847/1538-4357/aad0a0](https://doi.org/10.3847/1538-4357/aad0a0)
- Gray, R. O., Corbally, C. J., Garrison, R. F., et al. 2006, *AJ*, 132, 161, doi: [10.1086/504637](https://doi.org/10.1086/504637)
- Gray, R. O., Corbally, C. J., Garrison, R. F., McFadden, M. T., & Robinson, P. E. 2003, *AJ*, 126, 2048, doi: [10.1086/378365](https://doi.org/10.1086/378365)
- Guo, X., Johnson, J. A., Mann, A. W., et al. 2017, *ApJ*, 838, 25, doi: [10.3847/1538-4357/aa6004](https://doi.org/10.3847/1538-4357/aa6004)
- Haario, H., Laine, M., Mira, A., & Saksman, E. 2006, *Stat Comp.*, 16
- Hadden, S., & Lithwick, Y. 2017, *AJ*, 154, 5, doi: [10.3847/1538-3881/aa71ef](https://doi.org/10.3847/1538-3881/aa71ef)
- Henry, G. W. 1999, *PASP*, 111, 845, doi: [10.1086/316388](https://doi.org/10.1086/316388)
- Henry, G. W., Marcy, G., Butler, R. P., & Vogt, S. S. 1999, *IAUC*, 7307, 1
- Henry, G. W., Marcy, G. W., Butler, R. P., & Vogt, S. S. 2000, *ApJL*, 529, L41, doi: [10.1086/312458](https://doi.org/10.1086/312458)
- Hinkel, N. R., Mamajek, E. E., Turnbull, M. C., et al. 2017, *ApJ*, 848, 34, doi: [10.3847/1538-4357/aa8b0f](https://doi.org/10.3847/1538-4357/aa8b0f)
- Houdebine, E. R. 2012, *MNRAS*, 421, 3189, doi: [10.1111/j.1365-2966.2012.20649.x](https://doi.org/10.1111/j.1365-2966.2012.20649.x)
- Houdebine, É. R., Mullan, D. J., Doyle, J. G., et al. 2019, *AJ*, 158, 56, doi: [10.3847/1538-3881/ab23fe](https://doi.org/10.3847/1538-3881/ab23fe)
- Houdebine, E. R., Mullan, D. J., Paletou, F., & Gebran, M. 2016, *ApJ*, 822, 97, doi: [10.3847/0004-637X/822/2/97](https://doi.org/10.3847/0004-637X/822/2/97)

- Howard, A. W., Johnson, J. A., Marcy, G. W., et al. 2010, *ApJ*, 721, 1467, doi: [10.1088/0004-637X/721/2/1467](https://doi.org/10.1088/0004-637X/721/2/1467)
- Isaacson, H., & Fischer, D. 2010, *ApJ*, 725, 875, doi: [10.1088/0004-637X/725/1/875](https://doi.org/10.1088/0004-637X/725/1/875)
- Jenkins, J. M., Twicken, J. D., McCauliff, S., et al. 2016, *Society of Photo-Optical Instrumentation Engineers (SPIE) Conference Series*, Vol. 9913, The TESS science processing operations center, 99133E
- Kaminski, A., Trifonov, T., Caballero, J. A., et al. 2018, *A&A*, 618, A115, doi: [10.1051/0004-6361/201833354](https://doi.org/10.1051/0004-6361/201833354)
- Kass, & Raftery. 1995, "Journal of the American statistical association", 90
- Katz, D., Soubiran, C., Cayrel, R., et al. 2011, *A&A*, 525, A90, doi: [10.1051/0004-6361/201014840](https://doi.org/10.1051/0004-6361/201014840)
- Kazarovets, E. V., Kireeva, N. N., Samus, N. N., & Durlevich, O. V. 2003, *Information Bulletin on Variable Stars*, 5422, 1
- Kervella, P., Arenou, F., Mignard, F., & Thévenin, F. 2019, *A&A*, 623, A72, doi: [10.1051/0004-6361/201834371](https://doi.org/10.1051/0004-6361/201834371)
- Kóspál, Á., Ardila, D. R., Moór, A., & Ábrahám, P. 2009, *ApJL*, 700, L73, doi: [10.1088/0004-637X/700/2/L73](https://doi.org/10.1088/0004-637X/700/2/L73)
- Lalitha, S., Baroch, D., Morales, J. C., et al. 2019, *A&A*, 627, A116, doi: [10.1051/0004-6361/201935534](https://doi.org/10.1051/0004-6361/201935534)
- Latham, D. W., Rowe, J. F., Quinn, S. N., et al. 2011, *ApJL*, 732, L24, doi: [10.1088/2041-8205/732/2/L24](https://doi.org/10.1088/2041-8205/732/2/L24)
- Lépine, S., & Gaidos, E. 2011, *AJ*, 142, 138, doi: [10.1088/0004-6256/142/4/138](https://doi.org/10.1088/0004-6256/142/4/138)
- Lépine, S., Hilton, E. J., Mann, A. W., et al. 2013, *AJ*, 145, 102, doi: [10.1088/0004-6256/145/4/102](https://doi.org/10.1088/0004-6256/145/4/102)
- Liddle, A. R. 2007, *MNRAS*, 377, L74, doi: [10.1111/j.1745-3933.2007.00306.x](https://doi.org/10.1111/j.1745-3933.2007.00306.x)
- Lindgren, L., Hernández, J., Bombrun, A., et al. 2018, *A&A*, 616, A2, doi: [10.1051/0004-6361/201832727](https://doi.org/10.1051/0004-6361/201832727)
- Lissauer, J. J., Dawson, R. I., & Tremaine, S. 2014, *Nature*, 513, 336, doi: [10.1038/nature13781](https://doi.org/10.1038/nature13781)
- Lissauer, J. J., Ragozzine, D., Fabrycky, D. C., et al. 2011, *ApJS*, 197, 8, doi: [10.1088/0067-0049/197/1/8](https://doi.org/10.1088/0067-0049/197/1/8)
- Liu, F., Yong, D., Asplund, M., Ramírez, I., & Meléndez, J. 2016, *MNRAS*, 457, 3934, doi: [10.1093/mnras/stw247](https://doi.org/10.1093/mnras/stw247)
- Lockwood, G. W., Skiff, B. A., & Radick, R. R. 1997, *ApJ*, 485, 789, doi: [10.1086/304453](https://doi.org/10.1086/304453)
- Lodieu, N., Pérez-Garrido, A., Smart, R. L., & Silvotti, R. 2019, *A&A*, 628, A66, doi: [10.1051/0004-6361/201935533](https://doi.org/10.1051/0004-6361/201935533)
- López-Morales, M., Morrell, N. I., Butler, R. P., & Seager, S. 2006, *PASP*, 118, 1506, doi: [10.1086/508904](https://doi.org/10.1086/508904)
- Luck, R. E. 2017, *AJ*, 153, 21, doi: [10.3847/1538-3881/153/1/21](https://doi.org/10.3847/1538-3881/153/1/21)
- Luck, R. E., & Heiter, U. 2005, *AJ*, 129, 1063, doi: [10.1086/427250](https://doi.org/10.1086/427250)
- Mackereth, J. T., & Bovy, J. 2018, *PASP*, 130, 114501, doi: [10.1088/1538-3873/aadced](https://doi.org/10.1088/1538-3873/aadced)
- Mamajek, E. E., & Hillenbrand, L. A. 2008, *ApJ*, 687, 1264, doi: [10.1086/591785](https://doi.org/10.1086/591785)
- Mann, A. W., Feiden, G. A., Gaidos, E., Boyajian, T., & von Braun, K. 2015, *ApJ*, 804, 64, doi: [10.1088/0004-637X/804/1/64](https://doi.org/10.1088/0004-637X/804/1/64)
- Martín, E. L., Lodieu, N., Pavlenko, Y., & Béjar, V. J. S. 2018, *ApJ*, 856, 40, doi: [10.3847/1538-4357/aaae8](https://doi.org/10.3847/1538-4357/aaae8)
- Mayor, M., Pepe, F., Queloz, D., et al. 2003, *The Messenger*, 114, 20
- Meschiari, S., Wolf, A. S., Rivera, E., et al. 2009, *Publications of the ASP*, 121, 1016, doi: [10.1086/605730](https://doi.org/10.1086/605730)
- Mikolaitis, Š., Drazdauskas, A., Minkevičiūtė, R., et al. 2019, *A&A*, 628, A49, doi: [10.1051/0004-6361/201835004](https://doi.org/10.1051/0004-6361/201835004)
- Millholland, S., Wang, S., & Laughlin, G. 2017, *ApJL*, 849, L33, doi: [10.3847/2041-8213/aa9714](https://doi.org/10.3847/2041-8213/aa9714)
- Mishenina, T. V., Pignatari, M., Korotin, S. A., et al. 2013, *A&A*, 552, A128, doi: [10.1051/0004-6361/201220687](https://doi.org/10.1051/0004-6361/201220687)
- Mishenina, T. V., Soubiran, C., Bienaymé, O., et al. 2008, *A&A*, 489, 923, doi: [10.1051/0004-6361:200810360](https://doi.org/10.1051/0004-6361:200810360)
- Mishenina, T. V., Soubiran, C., Kovtyukh, V. V., Katsova, M. M., & Livshits, M. A. 2012, *A&A*, 547, A106, doi: [10.1051/0004-6361/201118412](https://doi.org/10.1051/0004-6361/201118412)
- Nelson, B. E., Ford, E. B., Buchner, J., et al. 2020, *AJ*, 159, 73, doi: [10.3847/1538-3881/ab5190](https://doi.org/10.3847/1538-3881/ab5190)
- Ning, B., Wolfgang, A., & Ghosh, S. 2018, *ApJ*, 869, 5, doi: [10.3847/1538-4357/aaeb31](https://doi.org/10.3847/1538-4357/aaeb31)
- Olsper, N., Lehtinen, J. J., Käpylä, M. J., Pelt, J., & Grigorievskiy, A. 2018, *A&A*, 619, A6, doi: [10.1051/0004-6361/201732525](https://doi.org/10.1051/0004-6361/201732525)
- Pepe, F., Mayor, M., Rupprecht, G., et al. 2002, *The Messenger*, 110, 9
- Pepe, F., Mayor, M., Queloz, D., et al. 2004, *A&A*, 423, 385, doi: [10.1051/0004-6361:20040389](https://doi.org/10.1051/0004-6361:20040389)
- Perryman, M. 2011, *The Exoplanet Handbook*
- Pinamonti, M., Sozzetti, A., Giacobbe, P., et al. 2019, *A&A*, 625, A126, doi: [10.1051/0004-6361/201834969](https://doi.org/10.1051/0004-6361/201834969)
- Quirrenbach, A., Amado, P. J., Caballero, J. A., et al. 2014, in *Society of Photo-Optical Instrumentation Engineers (SPIE) Conference Series*, Vol. 9147, Proc. SPIE, 91471F
- Quirrenbach, A., Amado, P. J., Ribas, I., et al. 2018, in *Society of Photo-Optical Instrumentation Engineers (SPIE) Conference Series*, Vol. 10702, Proc. SPIE, 107020W
- Radick, R. R., Lockwood, G. W., Skiff, B. A., & Baliunas, S. L. 1998, *ApJS*, 118, 239, doi: [10.1086/313135](https://doi.org/10.1086/313135)
- Rajpaul, V., Aigrain, S., & Roberts, S. 2016, *MNRAS*, 456, L6, doi: [10.1093/mnras/slv164](https://doi.org/10.1093/mnras/slv164)

- Ramírez, I., Fish, J. R., Lambert, D. L., & Allende Prieto, C. 2012, *ApJ*, 756, 46, doi: [10.1088/0004-637X/756/1/46](https://doi.org/10.1088/0004-637X/756/1/46)
- Rein, H., & Liu, S. F. 2012, *A&A*, 537, A128, doi: [10.1051/0004-6361/201118085](https://doi.org/10.1051/0004-6361/201118085)
- Rein, H., & Tamayo, D. 2015, *MNRAS*, 452, 376, doi: [10.1093/mnras/stv1257](https://doi.org/10.1093/mnras/stv1257)
- Reiners, A., Zechmeister, M., Caballero, J. A., et al. 2018, *A&A*, 612, A49, doi: [10.1051/0004-6361/201732054](https://doi.org/10.1051/0004-6361/201732054)
- Ricker, G. R., Winn, J. N., Vanderspek, R., et al. 2014, in *Society of Photo-Optical Instrumentation Engineers (SPIE) Conference Series*, Vol. 9143, Society of Photo-Optical Instrumentation Engineers (SPIE) Conference Series, 20
- Rowan, D., Meschiari, S., Laughlin, G., et al. 2016, *ApJ*, 817, 104, doi: [10.3847/0004-637X/817/2/104](https://doi.org/10.3847/0004-637X/817/2/104)
- Rowe, J. F., Bryson, S. T., Marcy, G. W., et al. 2014, *ApJ*, 784, 45, doi: [10.1088/0004-637X/784/1/45](https://doi.org/10.1088/0004-637X/784/1/45)
- Schweitzer, A., Passegger, V. M., Cifuentes, C., et al. 2019, *A&A*, 625, A68, doi: [10.1051/0004-6361/201834965](https://doi.org/10.1051/0004-6361/201834965)
- Slocum, F., & Mitchell, S. A. 1913, *ApJ*, 38, 1, doi: [10.1086/142012](https://doi.org/10.1086/142012)
- Smith, J. C., Stumpe, M. C., Van Cleve, J. E., et al. 2012, *PASP*, 124, 1000, doi: [10.1086/667697](https://doi.org/10.1086/667697)
- Soubiran, C., Jasniewicz, G., Chemin, L., et al. 2013, *A&A*, 552, A64, doi: [10.1051/0004-6361/201220927](https://doi.org/10.1051/0004-6361/201220927)
- Stassun, K. G., Oelkers, R. J., Pepper, J., et al. 2018, *AJ*, 156, 102, doi: [10.3847/1538-3881/aad050](https://doi.org/10.3847/1538-3881/aad050)
- Stassun, K. G., Oelkers, R. J., Paegert, M., et al. 2019, *AJ*, 158, 138, doi: [10.3847/1538-3881/ab3467](https://doi.org/10.3847/1538-3881/ab3467)
- Steffen, J. H., Ragozzine, D., Fabrycky, D. C., et al. 2012, *Proceedings of the National Academy of Science*, 109, 7982, doi: [10.1073/pnas.1120970109](https://doi.org/10.1073/pnas.1120970109)
- Stevens, D. J., Stassun, K. G., & Gaudi, B. S. 2017, *AJ*, 154, 259, doi: [10.3847/1538-3881/aa957b](https://doi.org/10.3847/1538-3881/aa957b)
- Stumpe, M. C., Smith, J. C., Catanzarite, J. H., et al. 2014, *PASP*, 126, 100, doi: [10.1086/674989](https://doi.org/10.1086/674989)
- Stumpe, M. C., Smith, J. C., Van Cleve, J. E., et al. 2012, *PASP*, 124, 985, doi: [10.1086/667698](https://doi.org/10.1086/667698)
- Suárez Mascareño, A., Rebolo, R., González Hernández, J. I., & Esposito, M. 2017, *MNRAS*, 468, 4772, doi: [10.1093/mnras/stx771](https://doi.org/10.1093/mnras/stx771)
- Takeda, G., Ford, E. B., Sills, A., et al. 2007, *ApJS*, 168, 297, doi: [10.1086/509763](https://doi.org/10.1086/509763)
- Teske, J. K., Wang, S., Wolfgang, A., et al. 2018, *AJ*, 155, 148, doi: [10.3847/1538-3881/aaab56](https://doi.org/10.3847/1538-3881/aaab56)
- Torres, G. 2010, *AJ*, 140, 1158, doi: [10.1088/0004-6256/140/5/1158](https://doi.org/10.1088/0004-6256/140/5/1158)
- . 2019, *ApJ*, 883, 105, doi: [10.3847/1538-4357/ab3a30](https://doi.org/10.3847/1538-4357/ab3a30)
- Tuomi, M., Jones, H. R. A., Barnes, J. R., et al. 2018, *AJ*, 155, 192, doi: [10.3847/1538-3881/aab09c](https://doi.org/10.3847/1538-3881/aab09c)
- Tuomi, M., Jones, H. R. A., Jenkins, J. S., et al. 2013, *A&A*, 551, A79, doi: [10.1051/0004-6361/201220509](https://doi.org/10.1051/0004-6361/201220509)
- Van Eylen, V., & Albrecht, S. 2015, *ApJ*, 808, 126, doi: [10.1088/0004-637X/808/2/126](https://doi.org/10.1088/0004-637X/808/2/126)
- Vanderburg, A., & Johnson, J. A. 2014, *PASP*, 126, 948, doi: [10.1086/678764](https://doi.org/10.1086/678764)
- Vican, L. 2012, *AJ*, 143, 135, doi: [10.1088/0004-6256/143/6/135](https://doi.org/10.1088/0004-6256/143/6/135)
- Vogt, S. S., Allen, S. L., Bigelow, B. C., et al. 1994, in *Society of Photo-Optical Instrumentation Engineers (SPIE) Conference Series*, Vol. 2198, *Instrumentation in Astronomy VIII*, ed. D. L. Crawford & E. R. Craine, 362
- Vogt, S. S., Radovan, M., Kibrick, R., et al. 2014, *Publications of the ASP*, 126, 359, doi: [10.1086/676120](https://doi.org/10.1086/676120)
- Vogt, S. S., Butler, R. P., Burt, J., et al. 2017, *AJ*, 154, 181, doi: [10.3847/1538-3881/aa8b61](https://doi.org/10.3847/1538-3881/aa8b61)
- Wang, S. 2017, *Research Notes of the American Astronomical Society*, 1, 26, doi: [10.3847/2515-5172/aa9be5](https://doi.org/10.3847/2515-5172/aa9be5)
- Wang, S., Addison, B., Fischer, D. A., et al. 2018, *AJ*, 155, 70, doi: [10.3847/1538-3881/aaa2fb](https://doi.org/10.3847/1538-3881/aaa2fb)
- Weiss, L. M., Marcy, G. W., Petigura, E. A., et al. 2018, *AJ*, 155, 48, doi: [10.3847/1538-3881/aa9ff6](https://doi.org/10.3847/1538-3881/aa9ff6)
- Winn, J. N. 2010, *Exoplanet Transits and Occultations*, 55–77
- Winn, J. N., & Fabrycky, D. C. 2015, *ARA&A*, 53, 409, doi: [10.1146/annurev-astro-082214-122246](https://doi.org/10.1146/annurev-astro-082214-122246)
- Wright, J. T., Marcy, G. W., Butler, R. P., & Vogt, S. S. 2004, *ApJS*, 152, 261, doi: [10.1086/386283](https://doi.org/10.1086/386283)
- Wright, N. J., Drake, J. J., Mamajek, E. E., & Henry, G. W. 2011, *ApJ*, 743, 48, doi: [10.1088/0004-637X/743/1/48](https://doi.org/10.1088/0004-637X/743/1/48)
- Zechmeister, M., Reiners, A., Amado, P. J., et al. 2018, *A&A*, 609, A12, doi: [10.1051/0004-6361/201731483](https://doi.org/10.1051/0004-6361/201731483)